Received: 4 September 2020 | Revised: 26 April 2021 | Accepted: 28 April 2021

DOI: 10.1096/fj.202002072RR

RESEARCH ARTICLE

THE FASEB JOURNAL

Endothelial cells from umbilical cord of women affected by gestational diabetes: A suitable in vitro model to study mechanisms of early vascular senescence in diabetes

Pamela Di Tomo[1,2] | Nicola Alessio[3] | Stefano Falone[4] | Laura Pietrangelo[2,5] | Paola Lanuti[2,5] | Valeria Cordone[6] | Silvano Junior Santini[4] | Nadia Di Pietrantonio[1,2] | Marco Marchisio[2,5] | Feliciano Protasi[2,5] | Natalia Di Pietro[1,2] | Gloria Formoso[2,5] | Fernanda Amicarelli[4] | Umberto Galderisi[3] | Assunta Pandolfi[1,2]

[1]Department of Medical and Oral Sciences and Biotechnologies, University "G. d'Annunzio" of Chieti-Pescara, Chieti, Italy

[2]Center for Advanced Studies and Technology - CAST (ex CeSI-MeT), University "G. d'Annunzio" of Chieti-Pescara, Italy

[3]Department of Experimental Medicine, University of Campania "L. Vanvitelli", Napoli, Italy

[4]Department of Life, Health and Environmental Sciences, University of L'Aquila, L'Aquila, Italy

[5]Department of Medicine and Aging Sciences, University "G. d'Annunzio" of Chieti-Pescara, Chieti, Italy

[6]Department of Biomedical and Specialist Surgical Sciences, University of Ferrara, Ferrara, Italy

Correspondence
Assunta Pandolfi, Department of Medical and Oral Sciences and Biotechnologies, University "G. d'Annunzio" of Chieti-Pescara, Center for Advanced Studies and Technology - CAST (ex CeSI-MeT), Room 421 - Chieti, 66100, Italy.
Email: assunta.pandolfi@unich.it

Funding information
POR FESR ABRUZZO 2014-2020, Grant/Award Number: 39 DPG013/12222017; Italian telethon ONLUS Foundation, Grant/Award Number: GGP19231; Italian MIUR, Grant/Award Number: PRIN #2015ZZR4W3; Italian Society of Nephrology (SIN), Grant/Award Number: 10122016

Abstract

Human umbilical cord endothelial cells (HUVECs) obtained from women affected by gestational diabetes (GD-HUVECs) display durable pro-atherogenic modifications and might be considered a valid in vitro model for studying chronic hyperglycemia effects on early endothelial senescence. Here, we demonstrated that GD- compared to C-HUVECs (controls) exhibited oxidative stress, altered both mitochondrial membrane potential and antioxidant response, significant increase of senescent cells characterized by a reduced NAD-dependent deacetylase sirtuin-1 (SIRT1) activity together with an increase in cyclin-dependent kinase inhibitor-2A (P16), cyclin-dependent kinase inhibitor-1 (P21), and tumor protein p53 (P53) acetylation. This was associated with the p300 activation, and its silencing significantly reduced the GD-HUVECs increased protein levels of P300 and Ac-P53 thus indicating a persistent endothelial senescence via SIRT1/P300/P53/P21 pathway. Overall, our data suggest that GD-HUVECs can represent an "endothelial hyperglycemic memory"

Abbreviations: ΔΨm, mitochondrial membrane potential; γ-H2AX, H2A histone family member X phosphorylated; AGEs, advanced glycation end-products; CAT, catalase; GD, gestational diabetes; GSH, glutathione reduced; GSSG, glutathione oxidized; HG, high glucose; HUVECs, human umbilical vein endothelial cells; NO, nitric oxide; Nrf2, nuclear factor erythroid 2-related factor 2; P16, cyclin-dependent kinase inhibitor-2A; P21, cyclin-dependent kinase inhibitor-1; P53, tumor protein p53; ROS, reactive oxygen species; SA β-gal, senescence-associated beta-galactosidase; SIRT1, sirtuin-1; SOD, superoxide dismutase; TBARS, thiobarbituric acid reactive substances; T2D, type 2 diabetes.

Pamela Di Tomo and Nicola Alessio equally contributed to this study.

model to investigate in vitro the early endothelium senescence in cells chronically exposed to hyperglycemia in vivo.

KEYWORDS

endothelium, gestational diabetes, mitochondria, oxidative stress, senescence

1 | INTRODUCTION

The prevalence of type 2 diabetes (T2D) increases with age[1] and an estimated 8% of the world's adult population that today is affected by T2D is predicted to dramatically increase in the coming years.[2] In diabetic patients the dysfunction of multiple organ systems happens similarly as it does during normal chronological aging, but in this pathological condition this frequently occurs at a younger age,[3-5] suggesting that T2D itself might represent a pro-aging state.[6]

Among the known comorbidities, cardiovascular complications represent the leading cause of morbidity and mortality among patients with T2D.[7] In particular, hyperglycemia together with several metabolic alterations, chronic inflammation and oxidative stress, by altering the endothelial functions, are suspected to represent the initial pathological changes triggering the mechanistic pathway linking T2D to the related cardiovascular complications. Therefore, although the pathological link between diabetes and atherosclerosis is firmly established, a better comprehension of the underlying mechanisms is of extreme relevance to find novel potential molecular targets.[8]

Today, it is known that vascular aging is accelerated in patients with diabetes.[9] In several animal models, chronic hyperglycemia can cause vascular cell senescence, as shown in the aortas of Zucker diabetic rats but also in streptozotocin diabetic mice, and more recently in the aortic endothelium of diabetic rats were detected senescence-associated beta-galactosidase (SA β-gal)-stained cells.[10-12]

Likewise, numerous in vitro studies demonstrated that elevated glucose levels increase the senescence and/or apoptosis both in endothelial cells and endothelial progenitor cells (EPCs). The mechanism of glucose-induced senescence is not clear, although potential candidates include mitochondrial dysfunction, oxidative and glycosative cellular stress, decreased Nitric Oxide (NO) bioavailability, and molecular pathways leading to the activation of P53-driven DNA damage responses.[10,13-20]

We previously demonstrated in vitro the potential atherogenic changes in HUVECs earlier exposed to the specific metabolic milieu of gestational diabetes, proving that endothelial cells exposed in vivo even transiently to hyperglycaemia, oxidative stress and inflammation exhibit durable pro-atherogenic modifications.[13] More recently, we demonstrated that in cultured HUVECs the cytotoxic effect of elevated glucose levels was associated with oxidative and glycosative cellular stress, increased glutathione oxidized/glutathione reduced (GSSG/GSH) ratio, and strong reduction in the catalase/superoxide dismutase (CAT/SOD) ratio, which is suggestive of an impairment of the superoxide anion/hydrogen peroxide ($\mathbf{O}_2^{\bullet -}/H_2O_2$) detoxification process.[21] According to existing literature, this could represent one of the major determinants of the vascular oxidative stress commonly observed both in hyperglycemic and aging states.[6,22,23]

Notably, it has also been shown that in vitro glucose-induced upregulation of oxidative stress markers persists in HUVECs exposed to a constant high glucose concentration long after glucose normalization, a phenomenon termed "endothelial hyperglycemic memory".[24-26] In addition, Schisano et al[15] demonstrated that in vitro glucose oscillations, more than constant high glucose, induce P53 activation and a metabolic memory in human endothelial cells. Also, several studies suggest that during hyperglycemia-induced oxidative stress P53 might perform its pro-senescence and pro-apoptotic functions by directly targeting mitochondria, leading to changes in mitochondrial membrane potential ($\Delta\Psi m$).[27-29]

Recently, Zhang and colleagues[30] demonstrated that high glucose, in an in vitro cellular model of transient hyperglycemia, enhanced intracellular ROS production, which in turn inhibited the expression and deacetylase activity of NAD-dependent deacetylase sirtuin-1 (SIRT1) and simultaneously increased the protein level of p300. Accordingly, the transcriptional activity of *P53* was increased, and the expression of P21, a downstream gene of *P53*, was activated, potentially leading to persistent endothelial senescence via SIRT1/P300/P53/P21 pathway.

Remarkably, we lately characterized the in vitro phenotype of HUVECs chronically exposed in vivo to a hyperglycemic environment during pregnancy, identifying permanent molecular modifications of cellular homeostasis eventually impacting on oxidative and nitro-oxidative stress, inflammatory phenotype, NO synthesis and bioavailability, and thus potentially leading in vivo to vascular insult and atherosclerosis.[13] Our findings indicated that endothelial cells exposed even transiently to in vivo hyperglycemia exhibit durable pro-atherogenic modifications, supporting the concept of "endothelial hyperglycemic memory".

Although latest evidences suggest that diabetes and aging lead to comparable vascular dysfunction by mutual molecular

mechanisms,[6,22,31-36] the role of early endothelium senescence in the pathogenesis of vascular complications in diabetes is not well defined so far.

Thus, the main aim of this study was to demonstrate that HUVECs obtained from gestational diabetes umbilical cord vessels exhibited an early senescence phenotype potentially mediated by the SIRT1/P300/P53/P21 pathway and associated to impaired antioxidant enzymatic defence, inefficient mitochondrial antioxidant response and to reduced cells viability.

2 | MATERIALS AND METHODS

2.1 | Antibodies

Abcam (Cambridge, UK) provided the following primary antibodies: anti-SIRT1 (cat. ab12193; dil. 1:500), anti-SOD1 (cat. ab16831; dil. 1:500), anti-SOD2 (cat. ab86087; dil. 1:1000), anti-CAT (cat. ab16731; dil. 1:2000), anti-P16INK4A (cat. ab54210, dil. 1:500), anti-phospho-Nrf2 (cat. ab180844, dil. 1:5000 for western blotting analysis; dil. 1:200 for cytometry analysis), and anti-β-actin (cat. ab8227; dil. 1:10 000). Anti-RB1 (cat. AV33212, dil. 1:1000) and anti-GAPDH (cat. G8795, dil. 1:10 000) were purchased from Sigma-Aldrich (MO, USA), anti-RB2/P130 (cat. R27020, dil. 1:500) from BD Biosciences (CA, USA); anti-P27KIP1 (cat. 3686, dil. 1:300), anti-P53 for cytometry analysis (cat. 2524, dil. 1:50), anti-Acetyl-P53 (cat. 2525, dil. 1:100) and anti-γ-H2AX (cat. 2577, dil. 1:600) were from Cell Signaling (MA, USA), while anti-P107 (cat. sc-318, dil. 1:200), anti-P53 for western blotting analysis (cat. sc-126, dil. 1:500), anti-P21CIP1 (cat. sc-397, dil. 1:200), and anti-p300 (cat. sc-585, dil. 1:100) were obtained from Santa Cruz Biotechnology (CA, USA). The HRP-conjugated goat anti-rabbit IgG secondary antibody (cat. PI1000, dil. 1:1000) was purchased from Vector Laboratories (Burlingame, USA).

2.2 | Clinical characteristic of cords donors and newborns

Umbilical cords were obtained from randomly selected healthy Caucasian mothers (Control, C) and mothers affected by Gestational Diabetes (GD) delivering by Chieti and Pescara Hospitals (Italy).

GD mothers, followed by the "Diabetes and Pregnancy Clinic" hosted by the same Hospital, were treated with diet only. All GD women were affected by gestational diabetes arisen during the second trimester of pregnancy; women with pre-gestational diabetes were excluded. All procedures were in agreement with the Declaration of Helsinki principles and with the ethical standards of the Institutional Committee on Human Experimentation (Reference Number: 1879/09COET). After approval of the protocol by the Institutional Review Board, signed informed consent was obtained from each participating subject. The characteristics of donors' Control (n = 10) and GD (n = 10) mothers together with the newborns are described in Table 1.

Both control and GD pregnant women who donated the cords were overweight before pregnancy without significant weight differences between groups.

Reference range for anthropometric and biochemical parameters were: Body Mass Index (BMI) < 18.5 Kg/m^2, underweight range; 18.5-24.9 Kg/m^2, normal range; 25.0-29.99 Kg/m^2 overweight range; ≥30.0 Kg/m^2 or higher, obesity range. Systolic Blood Pressure (SBP) < 140 mm Hg. Diastolic Blood Pressure (DBP) < 90 mm Hg; Oral Glucose Tolerance Test (OGTT): basal glycemia ≥ 92 mg/dL (≥5.2 mmol/L), 1 hour glycemia ≥ 180 mg/dL (≥10 mmol/L), 2 hours glycemia ≥ 153 mg/dL (≥8.5 mmol/L).

2.3 | HUVECs isolation and culture

The HUVECs' explants were obtained by enzymatic digestion using 1 mg/mL Collagenase 1A (cat. C9891, Sigma-Aldrich) according to the previously detailed method.[37] C- and GD-HUVECs were grown in normal glucose (5.5 mM) medium (DMEM/M199, ratio 1:1, cat. D6046 and M4530, respectively, Sigma-Aldrich) supplemented with 1% L-glutamine (cat. G7513, Sigma-Aldrich), 1% penicillin/streptomycin (cat. P4333, Sigma-Aldrich), 20% Fetal Bovine Serum (FBS, cat. 41A0045K, Life Technologies, Monza, Italy), 10 μg/mL heparin and 50 μg/mL Endothelial Cell Growth Factor (ECGF). For experiments, cells were used between the third and fifth passage in vitro using at least three different cellular strains (n = 3) obtained from umbilical cords of C- or GD-women for each experiment.

2.4 | Cell lysis extraction for enzymatic activity

C-HUVECs and GD-HUVECs (6-8 × 10^6 cells/mL) were lysed in 100 mM KH_2PO_4 (pH 7), 0.1% Triton X-100 (cat. P0662 and 23 472-9, respectively, from Sigma-Aldrich). Samples were centrifuged at 16 000*g* for 30 minutes at 4°C, and the supernatants were used for assessments of enzymatic activities and total protein concentration (cat. 500-0006, Bio-Rad Laboratories), with BSA used as the standard. All readings were carried out in triplicates, using a Lamba25 UV-VIS spectrophotometer (PerkinElmer, Waltham, MA, USA).

TABLE 1 The clinical characteristics of donors mothers control (C, n = 10) and with gestational diabetes (GD, n = 10) (A) and newborns (B)

(A)	Pregnant women characteristics	C-women	GD-women
	Age (years)	35.6 ± 7.24	34.4 ± 3.24
	Height (cm)	163.05 ± 6.3	162.9 ± 7.98
	Pre–gestational Weight (Kg)	66.84 ± 13.66	68 ± 8.14
	Post–gestational Weight (Kg)	72.93 ± 12.5	75.31 ± 7.29
	Maternal gestational weight gain (Kg)	6.1 ± 3.56	8.66 ± 3.86
	BMI pre–gestational (Kg/m^2)	25.27 ± 5.68	26.38 ± 2.6
	BMI post–gestational (Kg/m^2)	27.16 ± 5.23	28.06 ± 2.65
	OGTT gestational week	27.8 ± 2.48	24.8 ± 4.18
	SBP (mm/Hg)	110.37 ± 8.17	107.7 ± 5.42
	DBP (mm/Hg)	72.12 ± 8.04	68.3 ± 9.36
	OGTT values (mmol/L):		
	Basal glycemia	4.49 ± 0.22	5.1 ± 0.27*
	1 hour glycemia	7.97 ± 0.91	9.81 ± 1.4*
	2 hours glycemia	6.35 ± 1.09	8.48 ± 1.3*
(B)	**Newborns clinical characteristics**	**C-mother**	**GD-mother**
	Number (M/F)	10 (5/5)	10 (4/6)
	Birth Height (cm)	51.6 ± 1.67	50.57 ± 0.97
	Birth Weight (g)	3507.14 ± 599.43	3419 ± 412.65
	Gestational week at delivery	38.85 ± 1.57	38.5 ± 1.5

Note: Data are expressed as mean ± SD.

Abbreviations: BMI, body mass index; DBP, diastolic blood pressure; OGTT, oral glucose tolerance test; SBP, systolic blood pressure.

*$P < .05$.

TABLE 2 Primer pairs used for amplicon generation

mRNA	Forward	Reverse	Source
sod1	5′-AGGCATGTTGGAGACTTGGG-3′	5′-CCACAAGCCAAACGACTTCC-3′	Primer blast[a]
sod2	5′-GGACAAACCTCAGCCCTAAC-3′	5′-ACACATCAATCCCCAGCAGT-3′	41
cat	5′-AGGGGCCTTTGGCTACTTTG-3′	5′-ACCCGATTCTCCAGCAACAG-3′	42
sirt1	5′-GCAGATTAGTAGGCGGCTTG-3′	5′-TCTGGCATGTCCCACTATCA-3′	43
β-actin	5′- ATTGCCGACAGGATGCAGA-3′	5′-AGTACTTGCGCTCAGGAGGA-3′	44

[a]NM_000454.4.

2.5 | Measurement of CAT and SOD activity

The CAT (EC 1.11.1.6) activity was assayed by monitoring the decomposition of 10 mM H_2O_2 (cat. 21676-3, Sigma Aldrich) at 240 nm, as described by Aebi.[38] One unit was defined as 1 μM of H_2O_2 reduced/min at 25°C.

Total SOD (EC 1.15.1.1) activity was assayed in 50 mM $NaHCO_3$ buffer (pH 10.2), containing 25 mM EDTA and 0.1 M epinephrine bitartrate (cat. E4375, Sigma-Aldrich). SOD ability to inhibit the epinephrine auto-oxidation was monitored at 480 nm, according to Sun and Zigman.[39] One unit was defined as the amount of enzyme required to halve the rate of epinephrine autoxidation at 30°C. After assessing tSOD specific activity, lysates were treated with 1 mM KCN (cat. 207810, Sigma-Aldrich) to inactivate SOD1 and measure the SOD2 activity. SOD1 activity was calculated by subtraction (tSOD-SOD2).[40]

2.6 | RNA extraction and relative quantitative real-timePCR (RT-PCR)

RNA was extracted from C-HUVECs and GD-HUVECs by Ribospin kit (cat. 304-150, GeneAll Biotechnology CO., Ltd, Seoul, Korea), and contaminant DNA was degraded by Riboclear plus (cat. 313-150), following the supplier's recommendations (GeneAll Biotechnology CO., Ltd). The resulting RNA was used to obtain cDNA via reverse transcription (cat. NP100041, OriGene Technologies, Inc, Rockville, MD). The

cDNA was used (dil. 1:20-1:200) for the SensiFast SYBR-based PCR step (cat. BIO-92005, Bioline, London, UK) in an Applied Biosystems 7300 system (Thermo Fisher Scientific, Rockford, IL, USA). Custom primers were synthetized by IDT Integrated DNA Technologies (Coralville, IA, USA) (Table 2).[41-44] Amplification steps were set as follows: initial denaturation at 95°C for 2 minutes, and 40 cycles of 95°C for 5 seconds and 60°C for 30 seconds. In order to verify whether unspecific targets may be co-amplified, melting curves were always performed for all the primer pairs (95°C for 15 seconds, 60°C for 1 minute, 95°C for 15 seconds, and 60°C for 15 seconds). Gene expression was calculated by using the $2^{-\Delta\Delta Ct}$ method for relative quantitation, using β-actin as the reference mRNA and one of the C-HUVECs as the calibrator sample.[45] All samples were processed by analyzing three replicates.

2.7 | TBARS assay

Lipid peroxidation is one of the early biochemical events occurring upon high glucose stress.[46] Accordingly, lipid peroxidation-derived molecules were found to be increased in several organs of diabetes in vivo models,[47] as well as in cells and plasma of diabetic patients.[48,49] In our study, the levels of thiobarbituric acid reactive substances (TBARS) were determined according to the method described by Yagi,[50] using the TBARS Assay kit (cat. 10009055, Cayman Chemical, Ann Arbor, MI, USA). Briefly, C-HUVECs and GD-HUVECs were extracted (6×10^7 cells/mL) in PBS and the resulting samples were mixed with one volume of SDS. Then, Color Reagent was added to each sample in triplicates, as suggested by the supplier. The reaction mixtures were incubated for one hour in boiling water and centrifuged at 1600*g* for 10 minutes at 4°C. Supernatants were read at 532 nm by a Lambda25 spectrophotometer (PerkinElmer). TBARS concentrations of unknown samples were interpolated on a linear calibration curve that was obtained from pure malondialdehyde (MDA)-containing reactions (0-50 μM).

2.8 | Total protein extraction and Western blotting analysis

In order to detect CAT, SODs and SIRT1 proteins, whole extracts from C-HUVECs and GD-HUVECs (2×10^7 cells/mL) were obtained in RIPA buffer (cat. R0278, Sigma-Aldrich), which was supplemented (1% each) with protease inhibitors (cat. P8340, Sigma-Aldrich) and phosphatase inhibitors I and II (cat. P2850 and P5726, respectively, from Sigma-Aldrich). For the measurements of protein expression of cell-cycle regulators, cells were lysed in a buffer containing 0.1% Triton (Bio-Rad, CA, USA) for 30 minutes in ice. Then, after centrifugation at 16 000*g* for 30 minutes at 4°C, all supernatants were assayed for total protein content, by using the BCA Protein Assay Kit and bovine serum albumin (BSA) as the standard (cat. PR23225, Euroclone, Milan, Italy). Denatured samples (10-20 μg) were run in triplicates on polyacrylamide gels (12%), and protein bands were transferred onto polyvinylidene difluoride (PVDF) membranes by electrophoretic transfer.[51,52] Non-specific binding sites were blocked at room temperature for 1 hour with 5% (w/v) Blotting-Grade Blocker (cat. 170-6404, Bio-Rad Laboratories, Milan, Italy), in Tris-buffer saline containing 0.05% (v/v) Tween-20 (TBS-T, cat. P5927, Sigma-Aldrich). Membranes were incubated overnight with the primary antibodies diluted in TBS-T, and, then, with the peroxidase-conjugated secondary antibody for 2 hours. The images of the specific immune complexes were revealed, acquired, and analyzed by using Enhanced Chemi-luminescent Substrate Kit (cat. EMP001005, Euroclone), AllianceLD2 hardware (UVItec Limited, Cambridge, UK), Quantity One® 1-D analysis software (Bio-Rad, CA, USA) and Total Lab TL120 software (TotalLab, Newcastle upon Tyne, UK). β-actin or GAPDH were used as the loading control for data normalization.

2.9 | SIRT1 activity

GD- and C-cells were lysed (20 mM Tris-Cl, pH 7.4, 135 mM NaCl, 1.5 mM MgCl2, 1 mM EGTA, 10% glycerol, 1% Nonidet P-40) and proteins were immunoprecipitated with anti-SIRT1-conjugated protein A agarose beads (cat. ab7343 and ab193254, respectively, Abcam, Cambridge, UK). Briefly, the agarose beads were mixed with primary antibody for 4 hours at 4°C (15 μg of anti-SIRT1 antibody/mL of beads). The mixture was then centrifuged and washed with the aforementioned lysis buffer several times. After the last wash, cell lysates (3 mg of total proteins) were incubated overnight with the antibody-beads mixture. The immunocomplexes were centrifuged and washed, and the immunoprecipitates were directly used for the SIRT1 activity assay kit (cat. ab156065, Abcam, Cambridge, UK), according to supplier's instructions.[21,53] The reaction mixtures were prepared by mixing 17 μL $_{dd}H_2O$, 5 μL fluoro-substrate peptide, 5 μL NAD^+, 5 μL developer, and 13 μL test samples. Fluorescence (ex. 355 nm, em. 460 nm) was detected for 70 minutes, with 2 minutes intervals, in a Victor3 microplate reader (PerkinElmer, Waltham, MA, USA). The assays were performed with three replicates and the activity levels were normalized to the respective SIRT1 protein levels obtained for C and GD-HUVECs.

2.10 | Small interfering RNA (siRNA) transfection

Human p300 siRNA (cat. L-003486-00-0005) and non-targeted scrambled siRNA Pool (SCR, cat. D-001206-13-05) were obtained from GE Healthcare Dharmacon (Lafayette,

CO, USA). Briefly, HUVECs were transiently transfected with SCR or siRNA with Hiperfect (cat. 301705, Qiagen, Hilden, Germany) according to manufacturer's instructions, using Opti-MEM medium (cat. 51985034, Gibco, ThermoFisher). SCR or siRNA were used at the most effective concentration for C-HUVECs (20 nM) and GD-HUVECs (50 nM) among all those tested (10-75 nM) (data not shown). The efficiency of gene silencing, monitored as suppression of p300 protein level, was assessed after 48 hours by flow cytometry in C-HUVECs, C- HUVECstreatedwith 25 mM glucose (C-HG) and GD-HUVECs for total and acetylated P53 (Ac-P53) protein expression levels evaluation.

2.11 | Flow cytometry analysis

For all cytometric experiments, C- and GD-HUVECs were detached with 0.5% trypsin/0.2% EDTA solution (cat. 59418C, Sigma-Aldrich), centrifuged at 1500 rpm for 5 minutes and 5×10^5 cells/sample were resuspended in Phosphate Buffered Saline (PBS, cat. D8662, Sigma-Aldrich). Flow cytometry analysis was performed on a BD FACS Canto II flow cytometer or byImaging flow cytometry (ImageStream AMNIS, BD Biosciences). 1×10^4 events for each sample were analyzed using FACSDiva v 6.1.3, IDEAS software (BD Biosciences) and FlowJo 8.3.3 software (Tree Star Inc, Ashland, OR).

For ROS levels evaluation, the samples were incubated with CellROX Oxidative Stress Reagents (cat. C10444, Molecular Probes, Eugene, Oregon, USA) at 2.5 μMin PBS for 30 minutes at 37°C. As positive control for endogenous ROS production, C- and GD-HUVECs were incubated with 300 μM of H_2O_2 for 30 minutes before the assay.

To determine protein expression of p-Nrf2, p300, P53 total and acetylated (Ac-P53) the cells were permeabilized by Intrasure kit (cat. 641778, BD Biosciences), processed and incubated with anti-p-Nrf2, anti-P300, anti-P53, and anti-Ac-P53 primary antibody and then with secondary antibodyAlexa 488-conjugated (1:100, cat. A11034, Invitrogen, CA, USA) for 30 minutes at 4°C. For nucleus-protein co-localization, nuclear staining was performed by incubating the cells with 7-Aminoactinomycin D (7-AAD, 1:100, cat. A9400, Sigma-Aldrich) for 10 minutes at room temperature and all samples were analyzed by Imaging flow cytometry (ImageStream AMNIS by using IDEAS software, BD). The results are expressed as MFI (Mean Fluorescence Intensity) Ratio, calculated by dividing the MFI of positive events by the MFI of negative events (MFI of secondary antibody).

The mitochondrial membrane potential ($\Delta\Psi m$) was evaluated in C- and GD-HUVECs incubated with JC-1 fluorescent probe (20 μM, by kit cat. ab113850, Abcam) for 30 minutes at 37°C. To induce complete depolarization of mitochondria, the protonophore CCCP (100 μM, cat. C2759, Sigma-Aldrich) was added to both cell strains 2 hours before the JC-1 incubation.

2.12 | Transmission electron microscopy (TEM)

2.12.1 | Preparation of samples

Approximately 2×10^6 cells cultured in monolayers were prepared for TEM as previously described by Capone and colleagues.[54] Briefly, cells were detached from the dish with 0.5% trypsin/0.2% EDTA solution, centrifuged at 1200 rpm for 10 minutes, washed three times with PBS, fixed with 3.5% glutaraldehyde in 0.1 M sodium cacodylate (NaCaCO) buffer (pH 7.2) for 1 hour and stored at 4°C. For embedding, cells were post-fixed in 2% OsO_4 in the same buffer for 2 hours and block-stained in uranyl acetate replacement. Ultrathin sections (~50 nm) were cut using a Leica Ultracut R microtome (Leica Microsystem) with a Diatome diamond knife (Diatome Ltd.) and double-stained with uranyl acetate replacement and lead citrate. Sections were viewed in a FP 505 Morgagni Series 268D electron microscope (FEI Company), equipped with Megaview III digital camera and Soft Imaging System at 60 kV.

2.12.2 | Quantitative analyses by TEM

Data contained in Table 3 were collected from 3 independent experiments on HUVEC cells either C or GD. Micrographs from single cells were randomly collected and used for the following quantitative analyses:

a. Number of severely damaged mitochondria. Mitochondria with any or several of the following ultrastructural alterations were classified as severely damaged: (i) mitochondria with clear disruption of the external membrane; (ii) presence of internal vacuolization and/or disrupted internal cristae; (iii) mitochondria containing *myelin-figures* (see Boncompagni et al for more detail).[55] The number of severely damaged mitochondria was counted in micrographs taken at either 4400-7100× magnification, and their number was reported as percentage of the total number (sample size: C, n = 1628; GD, n = 1870).
b. Mitochondrial average size. In each cell, mitochondria area was counted using Soft Imaging System in micrographs taken at 14 000-18 000× magnification and were reported as $\mu m^2 \times 10^{-2}$ (sample size: C, n = 940; GD, n = 1184).
c. Accumulation of autophagic vacuoles. The percentages of cells with accumulation of vacuoles delimited by membranes and containing electron-dense material were determined in micrographs taken at either 4400-7100× magnification (sample size: C, n = 41; GD, n = 55).
d. Frequency of fragmented Golgi. The number of disorganised Golgi stacks was counted in each cell group in micrographs taken at 14 000-18 000× magnification and reported as percentage of total number of Golgi (sample size: C, n = 61; GD, n = 75).

TABLE 3 Quantitative analysis of ultrastructural alterations in control (C) and GD-HUVECs

	A	B	C	D	E
	Damaged mitochondria, % of total	**Mitochondria average size ($\mu m^2 \times 10^{-2}$)**	**Cells with autophagic vacuoles, % of total**	**Fragmented Golgi, % of total**	**Trans-Golgi cisterna width (nm)**
C	4.3 ± 1.0 (n = 1628)	12.6 ± 0.3 (n = 940)	21.8 ± 9.0 (n = 61)	29.7 ± 12.6 (n = 61)	34.1 ± 2.1 (n = 61)
GD	6.8 ± 1.6* (n = 1870)	14.4 ± 0.3* (n = 1184)	52.2 ± 5.7* (n = 75)	65.6 ± 18.2* (n = 75)	44.5 ± 2.8* (n = 75)

Note: Data are shown as mean ± SEM (*$P < .01$). Sample size: in Columns A and B n = number of mitochondria analyzed; in Columns C, D, and E n = number of cells analyzed.

e. Trans-Golgi cisterna width. The width of the lumen of Trans-Golgi cisterna was measured in electron micrographs taken at 18 000× magnification, using Soft Imaging System (sample size: C, n = 61; GD, n = 75).

2.12.3 | In situ senescence-associated acid beta galactosidase assay

3×10^3 cells for cm^2 were fixed using a solution of 2% formaldehyde and 0.2% glutaraldehyde for 5 minutes at RT. After that, cells were washed with PBS 1X (MicroGem, Italia) and then overnight incubated at 37°C with a staining solution (citric acid/phosphate buffer (pH 6), $K4Fe(CN)_6$, $K3Fe(CN)_6$, NaCl, $MgCl_2$) containing 1 mg/mL of X-Gal (GoldBio, MO, USA). The percentage of senescent cells was calculated by the number of blue, β-galactosidase-positive cells out of at least 500 cells in different microscope fields, as already reported.[56] Where not specified otherwise, all reagents were obtained from Sigma-Aldrich.

2.12.4 | Immunocytochemistry (ICC)

The cells were fixed in 4% formaldehyde solution for 15 minutes at RT. Then were incubated with antibody against γ-H2AX at 4°C, overnight. Afterward the cells were incubated with the FITC-conjugated secondary antibody, obtained from ImmunoReagents (NC, USA). Nuclear staining was performed by DAPI mounting medium (cat, ab104139, Abcam) and micrographs were taken under fluorescence microscope (Leica, Germany). The percentage γ-H2AX was calculated by counting at least 500 cells in different microscope fields.

2.13 | MTT assay and cell count

Cell proliferation was assessed by MTT colorimetric assay (cat. M5655, Sigma-Aldrich), according to the manufacturer's instructions, and cell count. For MTT assay, both C- and GD-HUVECs were seeded at a density of 5×10^3 cells/well in 96 well plates. After 48 hours a solution of MTT in PBS (0.5 mg/mL) was added to each well and the plate was incubated at 37°C for 3 hours. The MTT crystals were solubilized with DMSO (200 µL/well) and the spectrophotometric absorbance was measured at 540 nm by using a microplate reader (SpectraMAX 190, Molecular Devices, Sunnyvale, CA). For cell count, C- and GD-HUVECs were seeded at a density of 4×10^4 cells/well in 12 well plates. After 48 hours, cells were washed at least three times with PBS w/o Ca^{++} and Mg^{++}. Then, the cells were incubated with Trypsin-EDTA at 37°C, detached, resuspended in PBS, and diluted (1:1) in Trypan blue solution (cat. 93595, Fluka). The counts cell was carried out in triplicate for each condition using a Burker's chamber.

2.13.1 | Statistics

Data are presented as means ± standard deviation (SD) or standard error of mean (SEM), where indicated of *n* cell strains from C- or GD-HUVECs explants. Independent experiments were performed by using each different cell strain.

To detect statistically significant differences between C-HUVECs and GD-HUVEC strains and between the different treatments Student's t test or two-way ANOVA test followed by Tukey's multiple comparison test for post hoc comparisons was used. $P < .05$ were considered statistically significant.

Microsoft Excel 2007 and Sigmaplot v12 packages were used for data processing and/or visualization.

3 | RESULTS

3.1 | GD-HUVECs exhibited impaired antioxidant enzymatic defense and increased oxidative stress

We first evaluated the specific activities and expression of enzymes involved in the antioxidant defense system of the cells, which is known to be compromised by aging. As shown in Figure 1, our data revealed that GD-HUVECs exhibited a

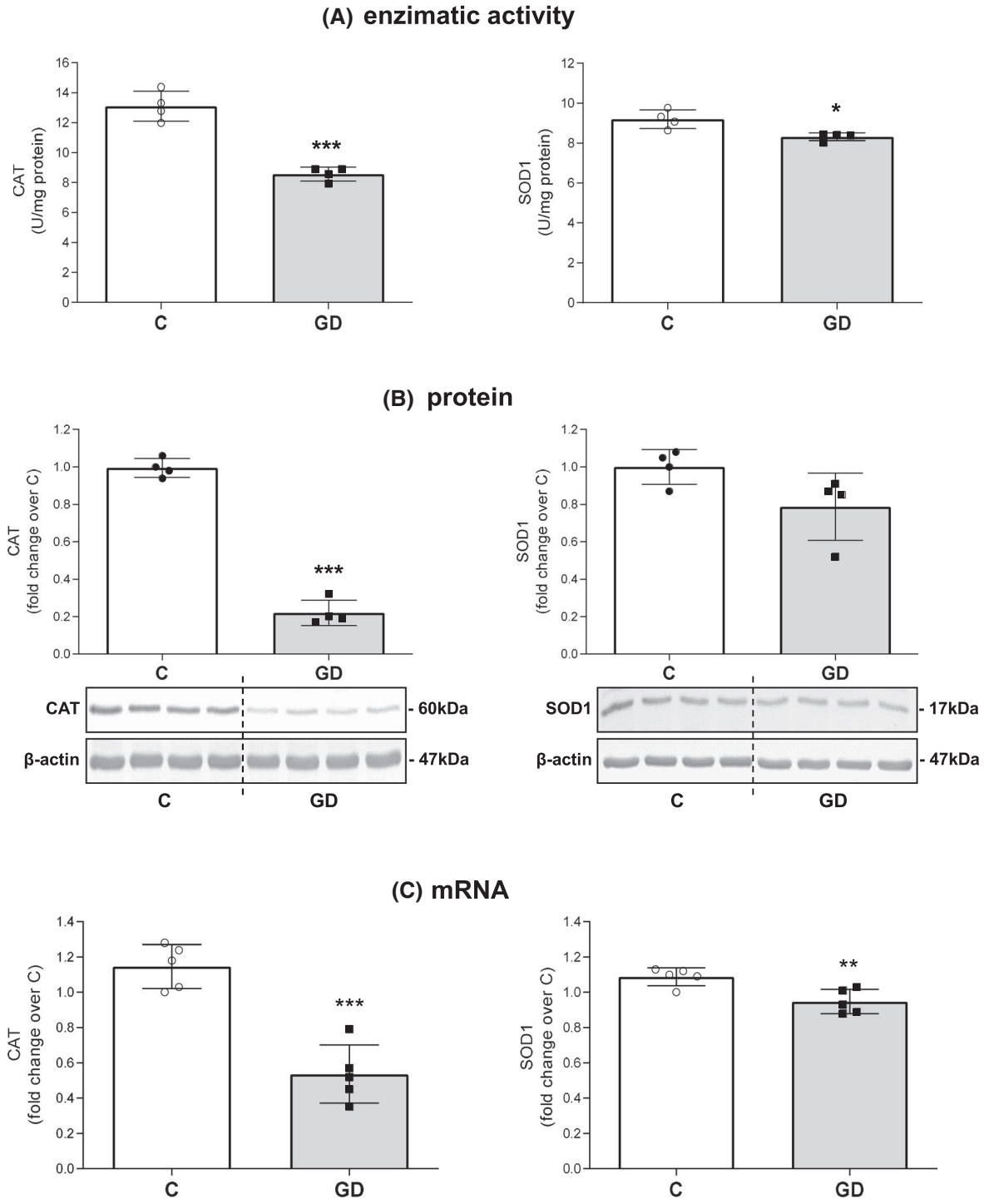

FIGURE 1 Impaired antioxidant enzymatic defence in GD-HUVECs, as compared to C-HUVECs. Scatter plots show enzymatic activity (A), protein level (B) and mRNA content (C) of CAT(left) and SOD1 (right). Data represent means ± SD of U/mg protein (A) and fold change over C-HUVECs (B and C). Gene expression (C) was calculated by using β-actin as the reference mRNA and one of the C-HUVECs as the calibrator sample. Representative Western blot images are also shown (B). Both C- and GD-HUVECs, n = 4 (A and B) n = 5 (C). *Student's* t *test*: **P* < .05, ***P* < .01 and ***P* < .001 versus C-HUVECs

statistically significant reduction in the activity of both catalase (CAT, $P < .001$) and superoxide dismutase 1 (SOD1, $P < .05$), as compared to C-HUVECs (Figure 1A). This was paralleled by similar decreases in protein levels of CAT ($P < .001$), whereas the reduction of SOD1 protein amount was found to be near significant ($P = .057$) (Figure 1B). Our analysis showed that the mRNAs coding for CAT and SOD1 were also both reduced in GD-HUVECs, with respect to C-HUVECs ($P < .001$ and $P < .01$ for CAT and SOD1, respectively) (Figure 1C).

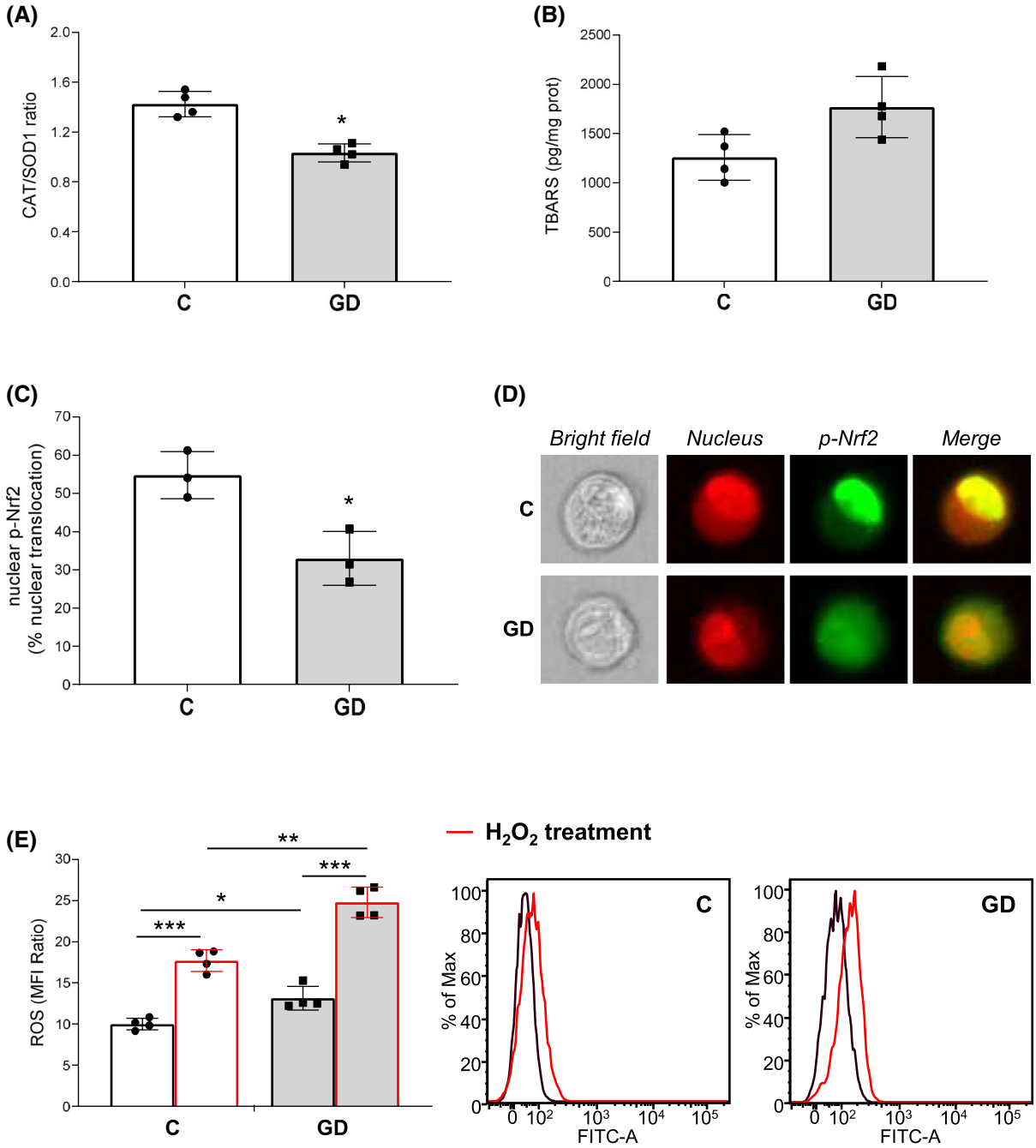

FIGURE 2 GD-HUVECs showed increased oxidative stress, as compared to C-HUVECs. Scatter plots in (A) and (B) show the ratio CAT/SOD1 activity and TBARS levels, respectively. In panel (C), data are expressed as percentage (%) of nuclear translocation of p-Nrf2. In the representative single cell images (D), nuclei are stained in red and p-Nrf2 in green for both C- and GD-HUVECs. Data represent means ± SD. Both C- and GD-HUVECs, n = 4 (A and B) and n = 3 (C and D). *Student's* t *test*:*$P < .05$ versus C-HUVECs. In (E) the scatter plot on the left shows the mean of data ± SD relating to the ROS production in C- and GD-HUVECs. Data are expressed as MFI Ratio. Both C- and GD-HUVECs, n = 4. On the right are shown the representative histograms obtained from the cytometric analysis. The red contours correspond to the treatment with 300 μM H_2O_2 for 30 minutes (positive control). *2-way ANOVA and Tukey's multiple comparison test*: *$P < .05$, **$P < .01$ and **$P < .001$

Of note, since the ratio of specific activities of coupled antioxidant enzymes better represents the overall efficiency of the anti-oxidative enzymatic defense than each activity alone,[57-59] we calculated the CAT over SOD1 ratio (Figure 2A) and we found that GD-HUVECs showed a strongly reduced CAT/SOD1 ratio, as compared to C-HUVECs ($P < .05$).

In addition, the thiobarbituric acid reactive substances (TBARS) levels found in GD-HUVECs were higher than those revealed in C-HUVECs (Figure 2B), although the differences did not reach statistical significance ($P = .057$).

We also observed that the nuclear translocation of phosphorylated Nuclear factor erythroid-2-related factor 2

(p-Nrf2), which is commonly observed upon its activation, has significantly decreased in GD-HUVECs, as compared to C-HUVECs ($P < .05$) (Figure 2C,D), although analysis of Nrf2 protein expression level shows no difference (1.01 ± 0.11 and 1.10 ± 0.19 arbitrary unit, C- and GD-HUVECs, respectively).

Finally, according to the impaired antioxidant enzymatic defense observed in GD-HUVECs, the cytometric analysis in Figure 2E demonstrated increased basal ROS levels in GD-HUVECs, as compared to C-HUVECs ($P < .05$), reinforcing all the findings above. As expected, upon exogenous pro-challenge (300 μM H_2O_2 for 30 minutes), ROS concentrations were found to be increased in both cell types ($P < .001$), even though ROS levels appeared significantly higher in GD- than in C-HUVECs ($P < .01$).

3.2 | GD-HUVECs showed inefficient mitochondrial antioxidant response and displayed ultrastructural and ΔΨm changes

High glucose is known to increase mitochondrial ROS production,[60] therefore we investigated whether gestational hyperglycemia in vivo could alter antioxidant defense within mitochondria. By comparing C- and GD-HUVECs, we found that the specific activity of SOD2 (ie, the mitochondrion-specific superoxide dismutase) was unchanged (2.66 ± 0.09 and2.66 ± 0.05 U/mg protein, C- and GD-HUVECs, respectively; $P = .88$), however we observed that SOD2 in GD cells was strongly up-regulated, mostly at transcriptional levels ($P < .01$ for SOD2 mRNA and $P < .05$ for SOD2 protein; Figure 3A,B, respectively). Also in this case, we calculated the CAT over SOD2 ratio, and we observed that GD-HUVECs showed a strongly reduced CAT/SOD2 ratio, as compared to C-HUVECs ($P < .01$; Figure 3C).

Additionally, the potential impairment of the mitochondrial system in GD-HUVECs was evaluated through the analysis of mitochondrial morphology (Figure 3D) and by measuring possible functional changes of ΔΨm (Figure 3E,F).

First, we observed mitochondria morphology in C- and GD-HUVECs at the ultrastructural level, using Transmission Electron Microscopy (TEM). Morphometric analysis indicated that although the number per area of these organelles was not significantly changed in GD-cells (27.1 ± 2.0/100 μm^2, n = 41 C-cells, versus 26.2 ± 1.7/100 μm^2, n = 55 GD-cells, $P = .726$), about 7% of mitochondria presented clear signs of damage, versus only about 4% in C-HUVECs (Table 3, column A). Moreover, even those mitochondria that are apparently normal, were significantly larger in size in GD- than in C-HUVECs (Figure 3D; and Table 3, column B), a possible indication of mitochondrial swelling in GD-cells. These findings suggest that chronic hyperglycemia, together with related oxidative stress and chronic inflammation, in endothelium might result in mitochondrial swelling and damage.

Successively, in order to determine the effects of the in vivo chronic hyperglycemia on mitochondrial function, we measured the changes of ΔΨm in both cell strains (Figure 3E,F). JC-1 staining was used to determine ΔΨm of the control and GD-cells. It is a lipophilic, cationic dye able to enter into the mitochondria where it accumulates forming reversible aggregates (yielding a red emission) in conditions of high mitochondrial potential. On the contrary, a decrease in membrane potential is associated with a reduction in aggregate formation and a prevalence of the JC-1 monomeric form (yielding a green emission).[61,62] The changes in ΔΨm were determined by detecting the red to green ratio of the fluorescence by JC-1 dye. The percentage of cells displaying JC1 red emission resulted down-regulated in GD- when compared to C-HUVECs, demonstrating a marked ΔΨm decrease in the GD than in control cells ($P < .05$, Figure 3E). As expected, the ΔΨm decreased markedly in both cell strains stressed by the protonophore CCCP (Figure 3F).

Notably, loss of ΔΨm has been highly correlated to the induction of senescence in different cell types,[63] thus these results suggest that chronic hyperglycemia in vivo may induce an early senescence in endothelial cells.

Furthermore, TEM examination of the overall ultrastructure of GD-cells revealed that, compared to control cells, GD-HUVECs contain more often autophagic vacuoles enclosing membranes or various electron-dense material (see Table 3, column C and empty arrows in Figure 4, panel B), a finding suggesting GD-cells possess dysregulated degradation pathways. This finding is consistent with investigations of senescent cells.[64]

Of note, in vivo chronic hyperglycemia seems also to cause other ultrastructural alterations in intracellular organelles: the Golgi membranes were often found fragmented and scattered throughout GD-cells (Table 3, column D and Figure 4, black arrows in panel D), in marked contrast to the ordered, ribbon-like structure they had in C-HUVECs (Table 3, column D and Figure 4, panel C). Moreover, measurement of the lumen of the Golgi cisternae indicated that GD-HUVECs had much wider Trans-Golgi cisternae (false-labeled in yellow in Figure 4, panels C and D) that are deputed to send cargoes forward to post-Golgi organelles (see Table 3, column E). All these findings are indicative of compromised Golgi integrity and interruption of the proper trafficking and processing of proteins that may be essential for GD-cell functions.

3.3 | GD-HUVECs exhibit senescence phenotype

After evaluating both the redox imbalance and the mitochondrial state, we sought to assess whether GD-HUVECs showed

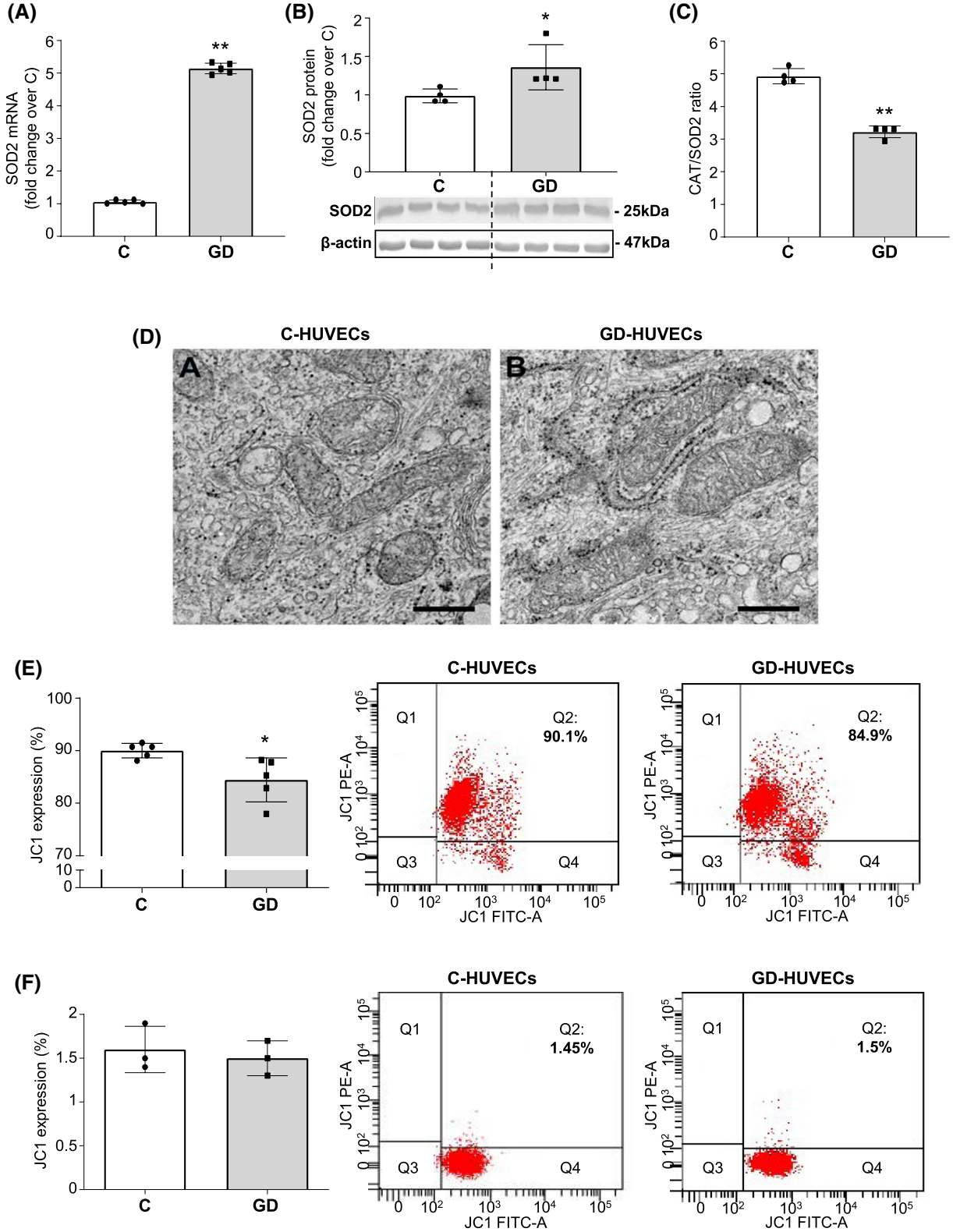

FIGURE 3 GD-HUVECs exhibited inefficient antioxidant response in mitochondria and displayed ultrastructural morphology and ΔΨm changes, as compared to C-HUVECs. Scatter plots show mRNA content (A) and protein level (B) of SOD2 and the ratio CAT/SOD2 activity (C). Data represent means ± SD of fold change over C-HUVECs. Both C- and GD-HUVECs, n = 5 (A) and n = 4 (B and C). *Student's* t-*test*: $*P < .05$ and $**P < .01$ versus C-HUVECs. Representative Western blot images are also shown (B). (D) Representative TEM micrograph of C-HUVECs (panel A) and GD-HUVECs (panel B) mitochondria. Scale bars: 500 nm. In (E) and (F) scatter plots and representative dot plots show the ΔΨm evaluation obtained from the cytometric analysis in C- and GD-HUVECs incubated with JC-1 fluorescent probe (E) and with the protonophore CCCP (F) to induce complete depolarization of mitochondria. The percentage shown in the quadrant Q2 corresponds to live C- and GD-cells with high mitochondrial potential in which JC1 is in aggregate form. Both C- and GD-HUVECs, n = 5 (E) and n = 3 (F). *Student's* t-*test*: $*P < .05$

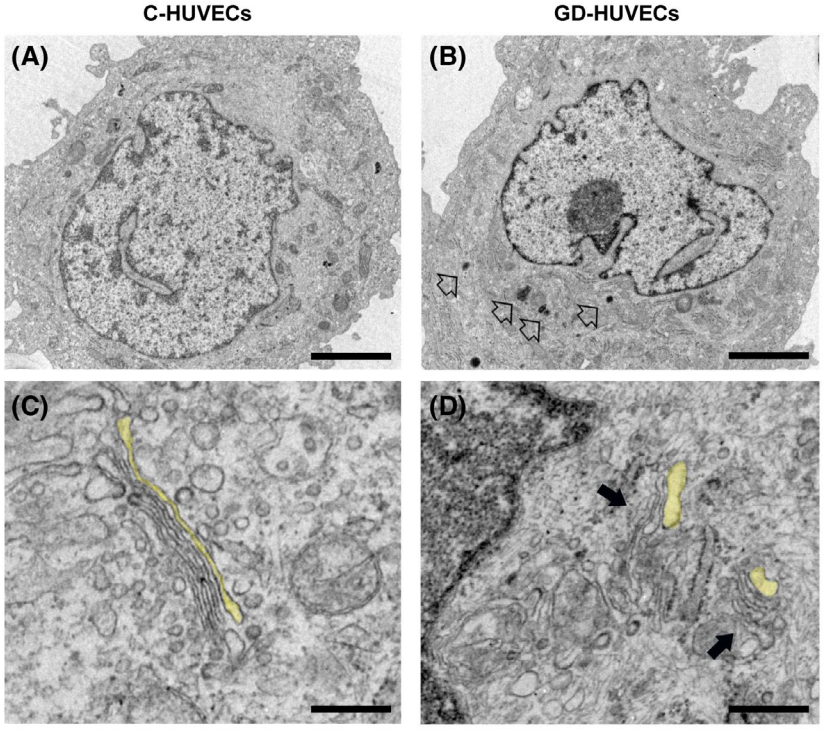

FIGURE 4 (A–B) Representative EM micrograph of C- and GD-HUVECs: in GD-cells, autophagic vacuoles containing membranes or various electron-dense material are often present (empty arrows in B). (C-D) Details at higher magnification of Golgi apparatus. The Trans-Golgi cisternae are false-labeled in yellow (C-D), while black arrows point to fragmented Golgi stacks (D). Scale bars: 2 μm (A and B); 0.4 μm (C and D)

onset of senescence process. Thus, we evaluated the percentage of senescent cells in both cell strains via β-galactosidase assay. Notably, in GD-HUVECs we detected a significant increase of senescent cells ($P < .01$; Figure 5A). This was associated with increased number of γ-H2AX foci, even though the statistical analysis could not exclude that the differences could be due to chance (Figure 5B).

Finally, as shown in Figure 5C, we also evaluated protein expression of cell-cycle regulators, such as those belonging to RB and P53 signaling. Interestingly, we observed a significant upregulation of P53, P21 and P16 protein levels in GD-cells, as compared to C-HUVECs ($P < .05$ for all). This expression pattern was associated with a reduction in RB expression ($P < .05$).

In parallel, MTT test (Figure 5D) and cell count (Figure 5E) confirm that GD-HUVECs show compromised proliferative potential demonstrating that GD-cells exhibited a slight but significant reduced viability[65] compared to control cells ($P \leq .05$ in D and E).

3.4 | GD-HUVECs showed an increase in P53 activity mediated by histone acetyltransferases p300

We then evaluated possible molecular mechanisms involved in the hyperglycemia-modulated acetylation levels of P53. Together with an increase in the P53 protein expression levels, we demonstrated that GD-HUVECs show significantly higher levels of acetylated P53 (Ac-P53) as compared to C-HUVECs ($P < .05$, Figure 6A). This has been associated with an increase in the total expression of the P300 protein (Figure 6B) and, interestingly, with an enhanced its nuclear localization (Figure 6C,D) in GD *versus* C-HUVECs ($P < .05$ for both), indicating its potential activation. Consistently with these results, the GD-HUVECs exhibited a reduced activity of sirtuin-1 (SIRT1; $P < .05$; Figure 6E), in spite of a significant increase of this protein both at translational ($P < .001$; Figure 6F) and transcriptional levels ($P < .05$; Figure 6G).

Next, to further investigate whether in our cellular model p300 potentially regulates the total and acetylation level of P53 at K382 in response to in vivo hyperglycemia possibly leading to a senescent phenotype, we transfected p300 siRNA both in GD-HUVECs and C-HUVECs treated or not with high glucose (25 mM for 48 hours; C-HG). In Figure 7A the data show that the transfection significantly reduced the protein levels of p300 both in GD-HUVECs ($P <.05$) and in C-HUVECs only after HG treatment ($P < .05$). In the same experimental condition, the *P300* silencing induced a significant decrease of P53 expression levels in GD-HUVECs ($P < .05$), which did not reached the statistical significance in C-HG-HUVEC (Figure 7B). Conversely, p300 siRNA transfection significantly reduced the levels of Ac-P53 in HG-treated HUVECs ($P < .05$) while induced a slight Ac-P53 decrease in GD-HUVECs (Figure 7C).

4 | DISCUSSION

Several reports suggest that chronic hyperglycemia together with related oxidative stress and chronic inflammation

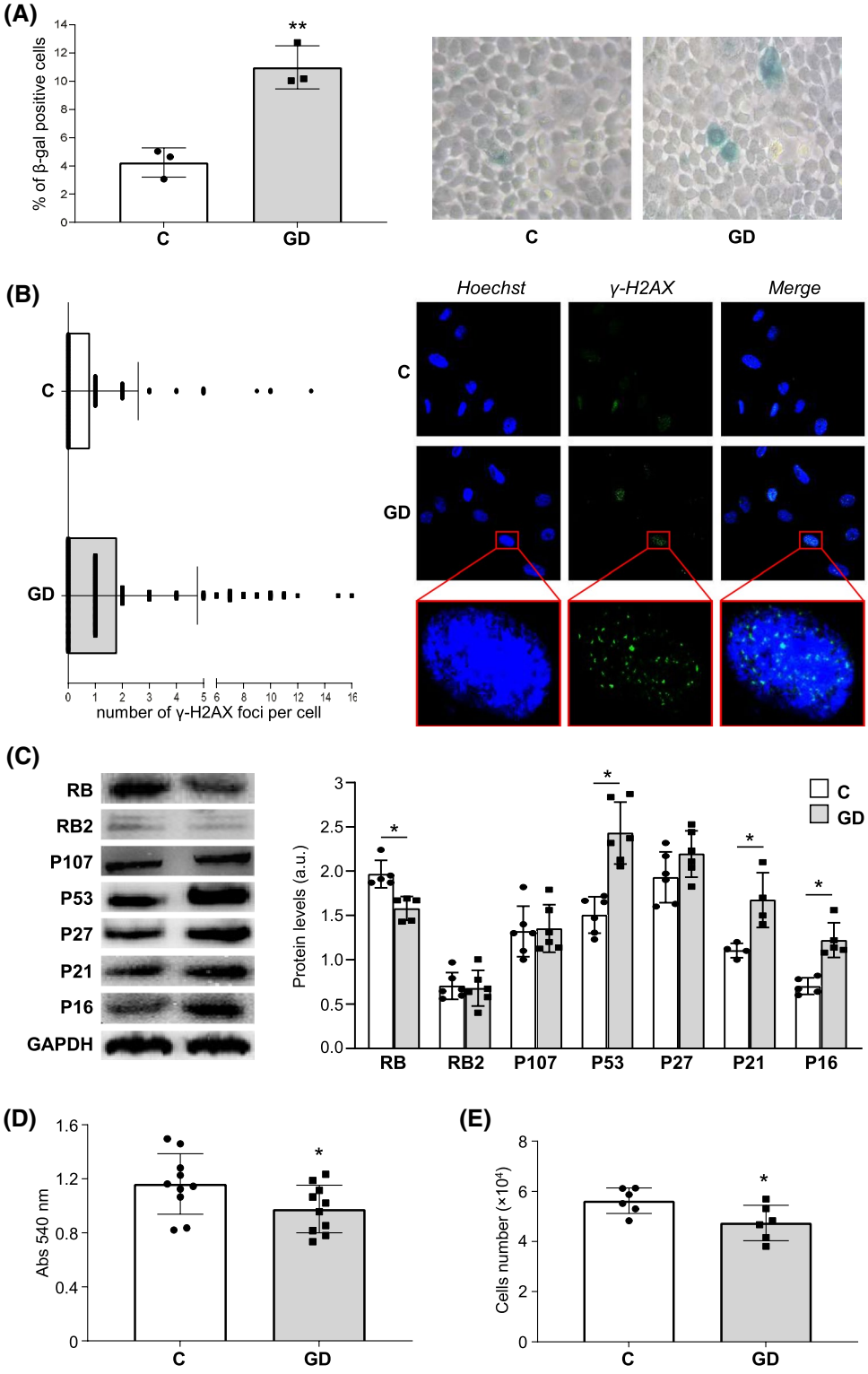

FIGURE 5 GD-HUVECs exhibit senescence phenotype, as compared to C-HUVECs. In (A) the scatter plot shows the percentage (%) of β-galactosidase positive cells; the representative images indicate the positive cells (blue cells) for acid β-galactosidase staining (400x). Data are expressed as mean ± SD. Both C- and GD-HUVECs, n = 3. *Student's* t-*test*: $^{**}P < .01$ versus C-HUVECs. B, The graph shows the degree of H2AX phosphorylation and each dot represents one cell. A representative microscopic field is shown (400x). The foci number was determined for 200 cells. C, The picture shows western blot analysis detection for the most protein involved in P16-RB and P21-P53 pathways. The histogram shows mean ± SD expression protein levels. Both C- and GD-HUVECs, n = 5. Histograms in (D) and (E) shown the proliferation level in C- and GD-HUVECs culture evaluated at 48 hours by MTT assay and cell number, respectively. Data are expressed as mean ± SD. Both C- and GD-HUVECs, n = 10 (D) and n = 6 (E). *Student's* t *test*: $^{*}P \leq .05$ versus C-HUVECs

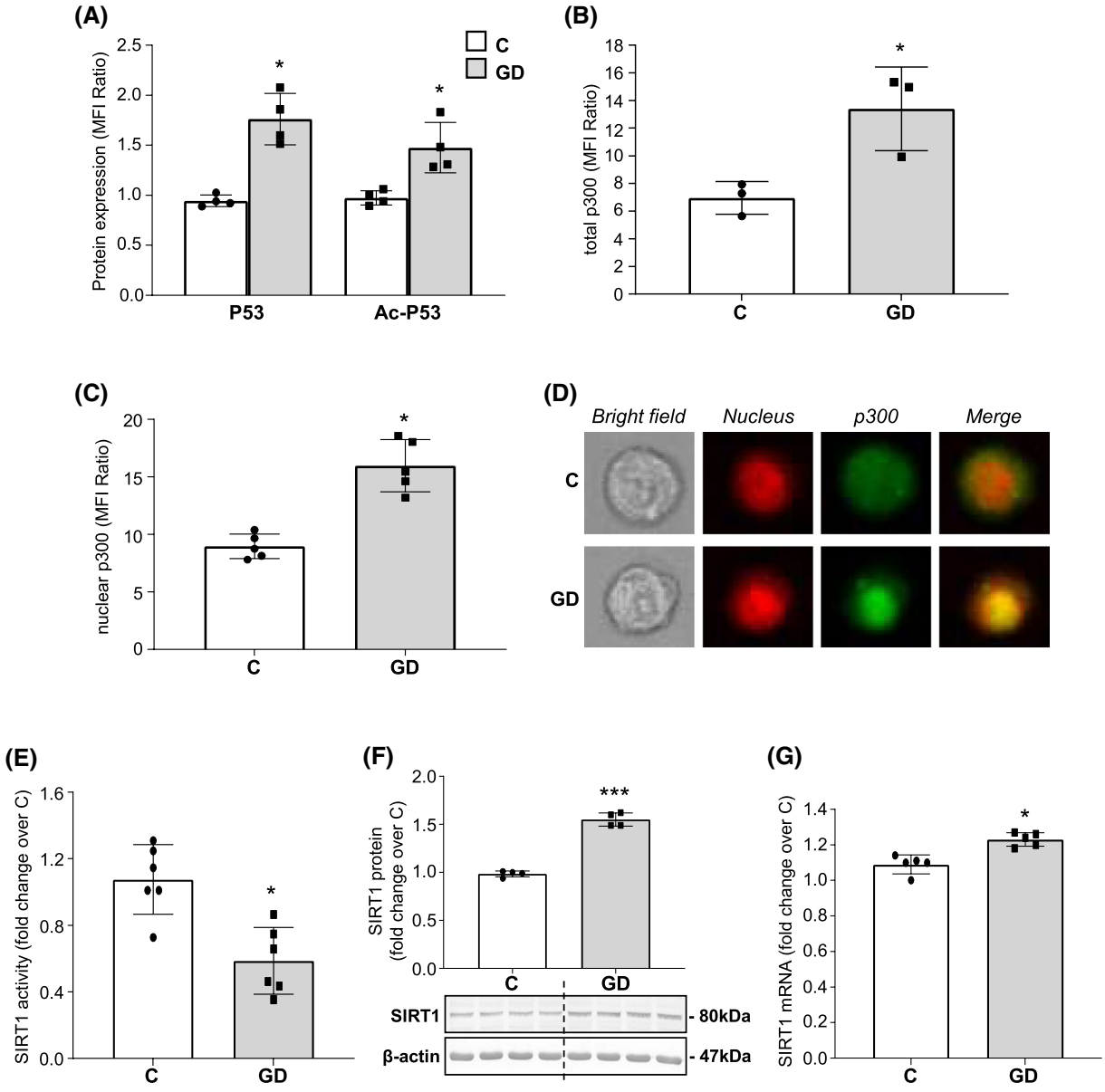

FIGURE 6 GD-HUVECs showed an increase in P53 acetylation (Ac-P53) mediated by p300/SIRT1 pathways, as compared to C-HUVECs. Scatter plots show total P53 and Ac-P53 (A), total p300 (B) and nuclear p300 (C) protein expression levels. Data represent means ± SD of MFI ratio. Both C- and GD-HUVECs, n = 4 (A), n = 3 (B) and n = 5 (C). *Student's* t *test*: **P* < .05 versus C-HUVECs. In the representative single cell images (D), nuclei are stained in red and p300 in green for both C- and GD-HUVECs. Scatter plots in panel (E), (F) and (G) show enzymatic activity, protein level and mRNA level of SIRT1, respectively. Data are expressed as means ± SD of fold change over C-HUVECs. Both C- and GD-HUVECs, n = 6 (E), n = 4 (F) and n = 5 (G). *Student's* t *test*: **P* < .05 and ****P* < .001 versus C-HUVECs. Representative Western blot images are also shown (F)

induces pro-atherogenic vascular modifications potentially correlated with early endothelium senescence,[8] nevertheless the mechanisms implicated in this phenomenon are not completely understood.

The mechanisms determining the development of endothelial dysfunction are complex and not limited to the solely hyperglycemia. Indeed, in pregnancies complicated by gestational diabetes and/or obesity, plasma concentration of circulating inflammatory molecules is increased, while plasma levels of anti-inflammatory molecules such as IL-10 and adiponectin are reduced[66] leading to an imbalance between pro- and anti-inflammatory/oxidative molecules. This condition may support the development of early vascular senescence and endothelial dysfunction,[67] then gestational diabetes may represent a suitable clinical model to study mechanisms underlying hyperglycemia-induced vascular damage.[68] Additionally, gestational diabetes is associated with a range of adverse perinatal and long-term outcomes for both mother

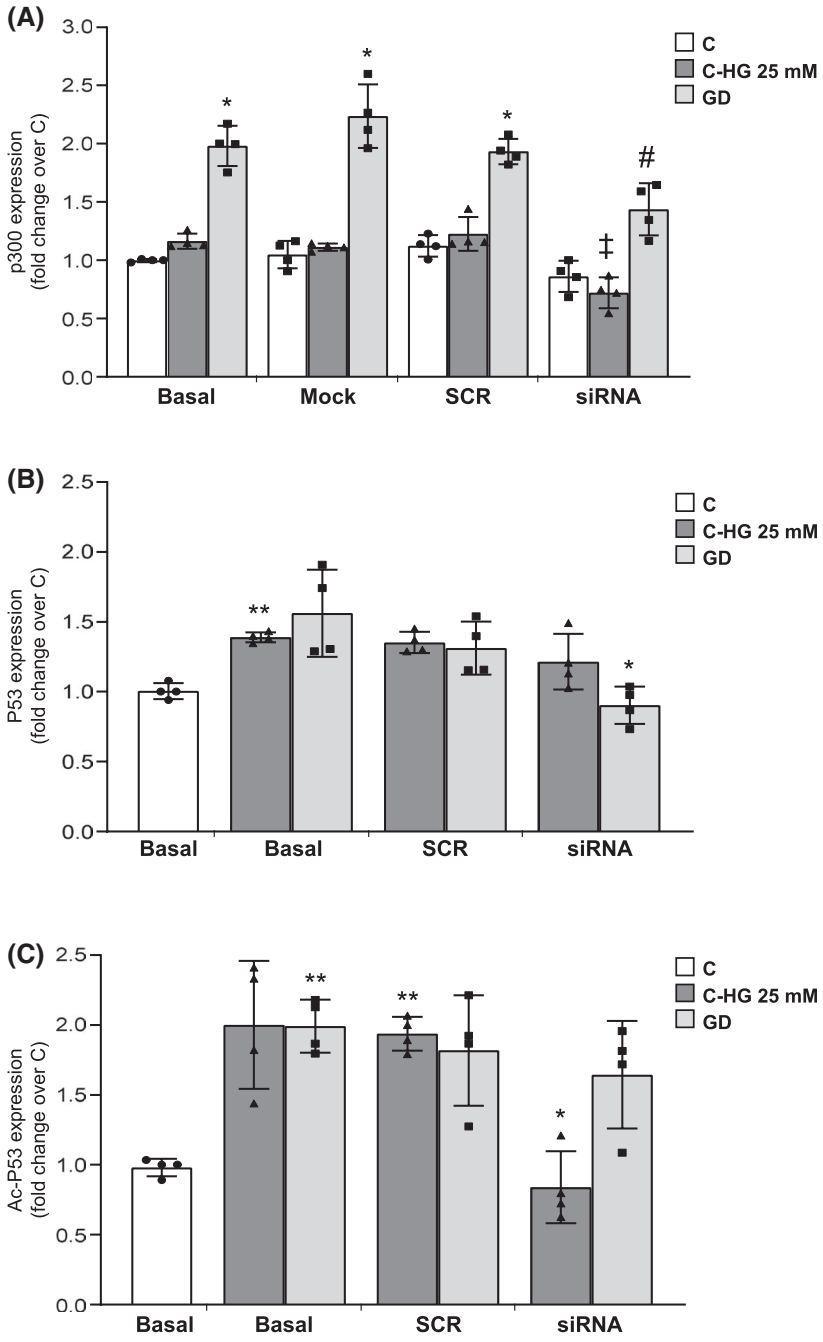

FIGURE 7 Transfection with p300 siRNA abolished the P53 expression in GD-HUVECs. In panel (A), the scatter plot shows p300 protein expression in transfected-HUVECs (48 hours) with human p300 siRNA, non-targeted scrambled siRNAs (SCR) or transfectant medium only (Mock), in GD-HUVECs and in C-cells treated (C-HG) or not (C) with glucose 25 mM for 48 hours. *2-way ANOVA and Tukey's multiple comparison test*: $*P < .05$ versus Basal C-HUVECs, $‡P < .05$ versus Basal, Mock and SCR C-HG-HUVECs, $\#P < .05$ versus Mock and SCR GD-HUVECs. Scatter plots in (B) and (C) show the protein level of total P53 andAc-P53, respectively, in non-transfected (Basal) C-, GD- and C-HG-HUVECs and transfected-cells with SCR or p300 siRNA in C-cellsafter stimulation with HG for 48 hours (C-HG) and GD-HUVECs. Data represent means ± SD andare expressed as fold change over C-Basal condition. For all C-, C-HG and GD-HUVECs, n = 4. *2-way ANOVA and Tukey's multiple comparison test*: $*P < .05$ versus Basal and SCR GD-HUVECs in (B) and versus Basal and SCR C-HG-HUVECs in (C), $**P < .01$ versus Basal C-HUVECs (B and C)

and offspring. In this perspective, epigenetic modifications are emerging as key players for the transmission of diabetic maternal phenotype to the offspring.

In support of this, we recently demonstrated that endothelial cells obtained from cords of Caucasian mothers affected by gestational diabetes and thus exposed in vivo to an altered metabolic milieu typical of diabetes seem to maintain a "diabetic cardiovascular phenotype" even after lengthy exposure in vitro to normal glucose levels configuring a sort of epigenetic control of gene expression. Notably, this would be consistent with the clinical data gathered in large outcome trials also pointing to the existence of a "metabolic legacy" due to an early exposure to a hyperglycemic environment which is "recorded" by the cells and may contribute to explain vascular complications observed in diabetic patients whose glycemic control has not been achieved very early.[13,24]

In the present study we employed several strains of human primary endothelial cells obtained from multiple donors affected by gestational diabetes, through which potentially hyperglycemia-modified mechanisms of early senescence could be studied without artefacts deriving from high glucose in vitro exposure.

Although this study was mainly focused on the GDM-associated fetoplacental endothelial dysfunction, it is interesting to mention that pregestational maternal obesity may associate with fetoplacental vascular alteration.[69] Thus, as

our study was not possible to separate the groups in pre-pregnancy maternal normal weight, overweight, and obesity this may represent a limitation of the present experimental design. However, further studies enrolling higher number of donors, might be aimed to understand if pregestational maternal overweight and/or obesity may influence GDM-associated fetoplacental endothelial dysfunction.

Today, it is largely accepted that vascular endothelial cell senescence is characterized by an increase of ROS, P53/P21, P16, SA-β-Gal, inflammatory response, and reduced nitric oxide (NO) bioavailability. All of them might have a pivotal role in the progression of cardiovascular complication in diabetes.[70]

We had previously shown that GD-cells exhibited an inflammatory imbalance associated with insulin resistance, increased superoxide anion ($O_2^{\bullet -}$) levels, and a reduced availability of NO.[13,71] The present study demonstrated the impairment of several molecular mechanisms that lead to premature endothelial senescence, suggesting that endothelium from umbilical cord of women affected by gestational diabetes may represent a suitable in vitro model to study mechanisms of early vascular senescence in diabetes.

In particular, GD- compared to C-HUVECs revealed an impaired antioxidant enzymatic defence (Figure 1), as well as increased basal and stimulated ROS levels associated with decreased nuclear localization of Nrf2 (Figure 2). These findings are consistent with data shown in recent studies in which the Nrf2 pathway, which is involved in anti-oxidative role inducing the gene expression of numerous antioxidant enzymes, appears to be compromised in endothelial cells exposed to maternal diabetes in utero.[32,33,72]

Interestingly, in our study the observed compromised antioxidant protection in GD-HUVECs was concomitant with an altered mitochondrial antioxidant response, ultrastructural mitochondrial changes, and the impairment of membrane potential (ΔΨm) (Figure 3). The latter is a sensitive indicator of the energetic state of the mitochondria, and can be used to assess the activity of the mitochondrial respiratory chain.[61,63] Maintenance of ΔΨm is required for the normal performance and survival of cells because of the high-energy requirement of cellular processes, such as cell growth.[73] In parallel with the impairment of ΔΨm, MTT test demonstrates that GD-cells exhibited a slight but significant reduced viability compared to control cells.[65] Additionally, all ultrastructural alterations in intracellular organelles shown in Figure 4 are indicative of compromised cell integrity that may be involved in onset and maintaining of endothelial senescence.[74]

It is accepted that mitochondrial dysfunction is quite often associated with chronic hyperglycemia and the changes in mitochondria leading to the generation of ROS are a part of the mechanism that triggers cell senescence by inducing both DNA damage and by translational and post–translational modifications of other macromolecules. The increase in ROS if not properly buffered by cell systems can lead to permanent modification of cell senescence phenotype.[34,75]

For this reason, we first decided to examine in our cellular model the senescence level by β-galactosidase assay and the degree of DNA damage by evaluating the expression level of phosphorylated histone H2AX and then to evaluate potential impairment of mechanisms involved in onset and senescence maintaining, such as RB and P53 pathways. In detail, the RB pathway is mainly associated with increase in P16 cyclin kinase inhibitor (CKI), while the P53 signaling relies on P21-P27 CKIs.[76]

As shown in Figure 5, the persistence of unrepaired DNA foci and increased percentage of β-galactosidase positive cells can be evidenced in GD-cells' nuclei, thus demonstrating an early senescent phenotype. Additionally, in these cells the senescence process appears mainly related to activation of P53. Indeed, we detected a strong increase in P53 expression with activation of P21. We found also an increase in P16 expression and a concomitant decrease of RB. This result is counterintuitive and need further investigation. On the other hand, in a previous finding, we demonstrated that senescence reliance on RB- and P53-related pathways is specie and cell type dependent.[77]

Finally, to assess the potential occurrence of metabolic memory of GD-endothelial cell senescence through SIRT1/P300/P53/P21 pathway we evaluated both SIRT1 and p300 activation since it is hypothesized that persistent down-regulation of deacetylase SIRT1 and up-regulation of acetyltransferase p300, may lead to sustained hyper-acetylation and activation of P53, and subsequent P53/P21-mediated "senescent memory"[30] (Figure 8).

Of note, reduced SIRT1 activity together with an increase in P53 acetylation determined by the p300 activation was demonstrated in GD- as compared to C-HUVECs (Figure 6) and, in agreement with data shown by Zhang and colleagues,[30] *P300* silencing reduced both the high glucose-increased protein levels of p300 and Ac-P53 in C-HUVECs and their elevated basal levels in GD-cells thus indicating a possible involvement of SIRT1/P300/P53/P21 pathway in the early senescent GD-HUVECs phenotype (Figures 7 and 8). In accordance with previous data from us and other authors,[21,78-81] we found that hyperglycemia induced a decrease in SIRT1 activity. However, we found that the decline in SIRT1 activity in GD-HUVECs was paralleled by an increase both at translational (Figure 6F) and transcriptional levels (Figure 6G). This may point to a possible attempt of a transcriptional and translational adaptive response occurring in GD-HUVECs exposed to a chronic hyperglycemia in vivo.

In conclusion, hypothesizing epigenetic changes, our data suggest that endothelial cells obtained from gestational

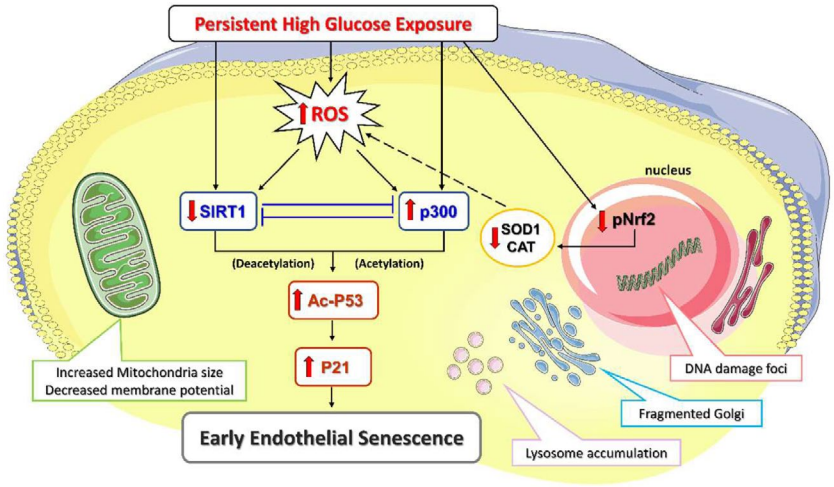

FIGURE 8 GD-HUVECs chronically exposed to hyperglycemia in vivo show early senescence phenotype in vitro. It is characterized by increased ROS levels, reduced CAT, SOD1, and Nrf2 activities. Decreased SIRT1 activity together within creased p300 levels result in increased acetylation of P53 and P21 expression. This is associated with the typical alterations of senescence including morphological and $\Delta\Psi m$ mitochondrial changes, increased DNA damage foci, fragmented Golgi, and lysosome accumulation

diabetes umbilical cord vessels can represent an innovative and suitable model to investigate in vitro the early endothelium senescence process that is experienced by cells chronically exposed to hyperglycemia in vivo (Figure 8). Notably, targeting fundamental vascular aging mechanisms could revolutionise the treatment of diabetes and have a major impact on the prevention of cardiovascular diabetic complications.

ACKNOWLEDGMENTS

This study was partially supported by grants from: POR FESR ABRUZZO 2014–2020 Asse I Determinazione (SANI, number: 39 DPG013/12222017) to Assunta Pandolfi; Italian Telethon ONLUS Foundation (GGP19231) and Italian MIUR (PRIN #2015ZZR4W3) to Feliciano Protasi; Italian Society of Nephrology (SIN, 10122016) to Natalia Di Pietro.

CONFLICT OF INTEREST

The authors have stated explicitly that there are no conflicts of interest in connection with this article.

AUTHOR CONTRIBUTIONS

A. Pandolfi, U. Galderisi, and F. Amicarelli designed and conceptualized the project, and wrote the manuscript. P. Di Tomo, N. Alessio, and S. Falone performed the experiments and wrote the manuscript. N. Di Pietrantonio performed the experiments and reviewed the manuscript. L. Pietrangelo and F. Protasi performed the electron microscopy experiments and reviewed the manuscript. P. Lanuti and M. Marchisio performed the flow cytometry experiments and reviewed the manuscript. V. Cordone and S. J. Santini provided technical support and reviewed the manuscript. N. Di Pietro and G. Formoso analyzed and interpreted the data, and reviewed the manuscript.

REFERENCES

1. Wild S, Roglic G, Green A, Sicree R, King H. Global prevalence of diabetes: estimates for the year 2000 and projections for 2030. *Diabetes Care*. 2004;27(5):1047-1053. https://doi.org/10.2337/diacare.27.5.1047
2. Guariguata L, Whiting DR, Hambleton I, Beagley J, Linnenkamp U, Shaw JE. Global estimates of diabetes prevalence for 2013 and projections for 2035. *Diabetes Res Clin Pract*. 2014;103(2):137-149. https://doi.org/10.1016/j.diabres.2013.11.002
3. Morley JE. Patient-centered care and cognitive dysfunction. *Clin Geriatr Med*. 2018;34(4):ix-x. https://doi.org/10.1016/j.cger.2018.08.013
4. Xu W, Caracciolo B, Wang H-X, et al. Accelerated progression from mild cognitive impairment to dementia in people with diabetes. *Diabetes*. 2010;59(11):2928-2935. https://doi.org/10.2337/db10-0539
5. Aronson D, Edelman ER. Coronary artery disease and DM. *Cardiol Clin*. 2015;32(3):439-455. https://doi.org/10.1016/j.ccl.2014.04.001
6. Palmer AK, Gustafson B, Kirkland JL, Smith U. Cellular senescence: at the nexus between ageing and diabetes. *Diabetologia*. 2019;62(10):1835-1841. https://doi.org/10.1007/s00125-019-4934-x
7. Domingueti CP, Dusse LMSA, Carvalho MDG, De Sousa LP, Gomes KB, Fernandes AP. Diabetes mellitus: The linkage between oxidative stress, inflammation, hypercoagulability and vascular complications. *J Diabetes Complications*. 2016;30(4):738-745. https://doi.org/10.1016/j.jdiacomp.2015.12.018
8. La Sala L, Prattichizzo F, Ceriello A. The link between diabetes and atherosclerosis. *Eur J Prev Cardiol*. 2019;26(2_suppl):15-24. https://doi.org/10.1177/2047487319878373
9. Hill MD. Stroke and diabetes mellitus. In: *Handbook of Clinical Neurology*. 2014;167-174. https://doi.org/10.1016/B978-0-444-53480-4.00012-6
10. Yokoi T, Fukuo K, Yasuda O, et al. Apoptosis signal-regulating kinase 1 mediates cellular senescence induced by high glucose in endothelial cells. *Diabetes*. 2006;55(6):1660-1665. https://doi.org/10.2337/db05-1607

11. Orimo M, Minamino T, Miyauchi H, et al. Protective role of SIRT1 in diabetic vascular dysfunction. *Arterioscler Thromb Vasc Biol*. 2009;29(6):889-894. https://doi.org/10.1161/ATVBAHA.109.185694
12. Hayashi T, Kotani H, Yamaguchi T, et al. Endothelial cellular senescence is inhibited by liver X receptor activation with an additional mechanism for its atheroprotection in diabetes. *Proc Natl Acad Sci USA*. 2014;111(3):1168-1173. https://doi.org/10.1073/pnas.1322153111
13. Di Fulvio P, Pandolfi A, Formoso G, et al. Features of endothelial dysfunction in umbilical cord vessels of women with gestational diabetes. *Nutr Metab Cardiovasc Dis*. 2014;24(12):1337-1345. https://doi.org/10.1016/j.numecd.2014.06.005
14. Kuki S, Imanishi T, Kobayashi K, Matsuo Y, Obana M, Akasaka T. Hyperglycemia accelerated endothelial progenitor cell senescence via the activation of p38 mitogen-activated protein kinase. *Circ J*. 2006;70(8):1076-1081. https://doi.org/10.1253/circj.70.1076
15. Schisano B, Tripathi G, McGee K, McTernan PG, Ceriello A. Glucose oscillations, more than constant high glucose, induce p53 activation and a metabolic memory in human endothelial cells. *Diabetologia*. 2011;54(5):1219-1226. https://doi.org/10.1007/s00125-011-2049-0
16. Yiu KH, Tse HF. Specific role of impaired glucose metabolism and diabetes mellitus in endothelial progenitor cell characteristics and function. *Arterioscler Thromb Vasc Biol*. 2014;34(6):1136-1143. https://doi.org/10.1161/ATVBAHA.114.302192
17. Ksiazek K, Passos JF, Olijslagers S, von Zglinicki T. Mitochondrial dysfunction is a possible cause of accelerated senescence of mesothelial cells exposed to high glucose. *Biochem Biophys Res Commun*. Published online. 2008;366(3):793-799. https://doi.org/10.1016/j.bbrc.2007.12.021
18. Yokoyama M, Shimizu I, Nagasawa A, et al. P53 plays a crucial role in endothelial dysfunction associated with hyperglycemia and ischemia. *J Mol Cell Cardiol*. 2019;129(February):105-117. https://doi.org/10.1016/j.yjmcc.2019.02.010
19. Navarrete Santos A, Jacobs K, Simm A, Glaubitz N, Horstkorte R, Hofmann B. Dicarbonyls induce senescence of human vascular endothelial cells. *Mech Ageing Dev*. 2017;166(June):24-32. https://doi.org/10.1016/j.mad.2017.07.009
20. Nigro C, Leone A, Fiory F, et al. Dicarbonyl stress at the crossroads of healthy and unhealthy aging. *Cells*. 2019;8(7):749. https://doi.org/10.3390/cells8070749
21. Santini, Cordone, Mijit, et al. SIRT1-dependent upregulation of antiglycative defense in HUVECs is essential for resveratrol protection against high glucose stress. *Antioxidants*. 2019;8(9):1-23. https://doi.org/10.3390/antiox8090346
22. Conti V, Corbi G, Simeon V, et al. Aging-related changes in oxidative stress response of human endothelial cells. *Aging Clin Exp Res*. 2015;27(4):547-553. https://doi.org/10.1007/s40520-015-0357-9
23. Donato AJ, Machin DR, Lesniewski LA. Mechanisms of dysfunction in the aging vasculature and role in age-related disease. *Circ Res*. Published online. 2018;123(7):825-848. https://doi.org/10.1161/CIRCRESAHA.118.3125-63
24. Coco C, Sgarra L, Potenza MA, et al. Can epigenetics of endothelial dysfunction represent the key to precision medicine in type 2 diabetes mellitus? *Int J Mol Sci*. 2019;20(12):1-26. https://doi.org/10.3390/ijms20122949
25. Ihnat MA, Thorpe JE, Kamat CD, et al. Reactive oxygen species mediate a cellular "memory" of high glucose stress signalling. *Diabetologia*. 2007;50(7):1523-1531. https://doi.org/10.1007/s00125-007-0684-2
26. Ceriello A, Ihnat MA, Thorpe JE. The "Metabolic memory": Is more than just tight glucose control necessary to prevent diabetic complications? *J Clin Endocrinol Metab*. 2009;94(2):410-415. https://doi.org/10.1210/jc.2008-1824
27. Chipuk JE, Green DR. PUMA cooperates with direct activator proteins to promote mitochondrial outer membrane permeabilization and apoptosis. *Cell Cycle*. Published online. 2009;8(17):2692-2696. https://doi.org/10.4161/cc.8.17.9412
28. Zhao Y, Chaiswing L, Velez JM, et al. P53 translocation to mitochondria precedes its nuclear translocation and targets mitochondrial oxidative defense protein-manganese superoxide dismutase. *Cancer Res*. 2005;65(9):3745-3750. https://doi.org/10.1158/0008-5472.CAN-04-3835
29. Ortega-Camarillo C, Guzmán-Grenfell AM, García-Macedo R, et al. Hyperglycemia induces apoptosis and p53 mobilization to mitochondria in RINm5F cells. *Mol Cell Biochem*. Published online. 2006;281(1-2):163-171. https://doi.org/10.1007/s11010-006-0829-5
30. Zhang E, Guo Q, Gao H, Xu R, Teng S, Wu Y. Metformin and resveratrol inhibited high glucose-induced metabolic memory of endothelial senescence through SIRT1/p300/p53/p21 pathway. *PLoS One*. 2015;10(12):1-19. https://doi.org/10.1371/journal.pone.0143814
31. Angulo J, El Assar M, Sevilleja-Ortiz A, et al. Short-term pharmacological activation of Nrf2 ameliorates vascular dysfunction in aged rats and in pathological human vasculature. A potential target for therapeutic intervention. *Redox Biol*. 2019;26:101271. https://doi.org/10.1016/j.redox.2019.101271
32. Cheng X, Chapple SJ, Patel B, et al. Gestational diabetes mellitus impairs nrf2-mediated adaptive antioxidant defenses and redox signaling in fetal endothelial cells in utero. *Diabetes*. 2013;62(12):4088-4097. https://doi.org/10.2337/db13-0169
33. Ganesh Yerra V, Negi G, Sharma SS, Kumar A. Potential therapeutic effects of the simultaneous targeting of the Nrf2 and NF-κB pathways in diabetic neuropathy. *Redox Biol*. 2013;1(1):394-397. https://doi.org/10.1016/j.redox.2013.07.005
34. Pandolfi A, De Filippis EA. Chronic hyperglicemia and nitric oxide bioavailability play a pivotal role in pro-atherogenic vascular modifications. *Genes Nutr*. 2007;2(2):195-208. https://doi.org/10.1007/s12263-007-0050-5
35. Jia G, Aroor AR, Jia C, Sowers JR. Endothelial cell senescence in aging-related vascular dysfunction. *Biochim Biophys Acta Mol Basis Dis*. Published online. 2019;1865(7):1802-1809. https://doi.org/10.1016/j.bbadis.2018.08.008
36. El Assar M, Angulo J, Santos-Ruiz M, et al. Asymmetric dimethylarginine (ADMA) elevation and arginase up-regulation contribute to endothelial dysfunction related to insulin resistance in rats and morbidly obese humans. *J Physiol*. 2016;594(11):3045-3060. https://doi.org/10.1113/JP271836
37. Di Tomo P, Lanuti P, Di Pietro N, et al. Liraglutide mitigates TNF-α induced pro-atherogenic changes and microvesicle release in HUVEC from diabetic women. *Diabetes Metab Res Rev*. 2017;33(8):e2925. https://doi.org/10.1002/dmrr.2925
38. Aebi H. Catalase in vitro. *Methods Enzymol*. Published online. 1984;105:121-126. https://doi.org/10.1016/S0076-6879(84)05016-3
39. Sun M, Zigman S. An improved spectrophotometric assay for superoxide dismutase based on epinephrine autoxidation.

Anal Biochem. Published online. 1978;90(1):81-89. https://doi.org/10.1016/0003-2697(78)90010-6

40. Bonfigli A, Colafarina S, Falone S, Di Giulio C, Di Ilio C, Amicarelli F. High levels of antioxidant enzymatic defence assure good protection against hypoxic stress in spontaneously diabetic rats. *Int J Biochem Cell Biol*. Published online. 2006;38(12):2196-2208. https://doi.org/10.1016/j.biocel.2006.06.011
41. Pluvinet R, Olivar R, Krupinski J, et al. CD40: An upstream master switch for endothelial cell activation uncovered by RNAi-coupled transcriptional profiling. *Blood*. Published online. 2008. https://doi.org/10.1182/blood-2008-03-143305
42. Patel H, Chen J, Das KC, Kavdia M. Hyperglycemia induces differential change in oxidative stress at gene expression and functional levels in HUVEC and HMVEC. *Cardiovasc Diabetol*. Published online. 2013;12(1):142. https://doi.org/10.1186/1475-2840-12-142
43. Herbert KJ, Cook AL, Snow ET. SIRT1 inhibition restores apoptotic sensitivity in p53-mutated human keratinocytes. *Toxicol Appl Pharmacol*. Published online. 2014;277(3):288-297. https://doi.org/10.1016/j.taap.2014.04.001
44. Yu YX, Gu ZL, Yin JL, et al. Ursolic acid induces human hepatoma cell line SMMC-7721 apoptosis via p53-dependent pathway. *Chin Med J (Engl)*. Published online. 2010;123:1915-1923. https://doi.org/10.3760/cma.j.issn.0366-6999.2010.14.016
45. Livak KJ, Schmittgen TD. Analysis of relative gene expression data using real-time quantitative PCR and the 2-ΔΔCT method. *Methods*. Published online. 2001;25(4):402-408. https://doi.org/10.1006/meth.2001.1262
46. Ha H, Yoon SJ, Kim KH. High glucose can induce lipid peroxidation in the isolated rat glomeruli. *Kidney Int*. 1994;46(6):1620-1626. https://doi.org/10.1038/ki.1994.461
47. Maritim AC, Sanders RA, Watkins JB. Diabetes, oxidative stress, and antioxidants: A review. *J Biochem Mol Toxicol*. Published online. 2003;17(1):24-38. https://doi.org/10.1002/jbt.10058
48. Rajeswari P, Natarajan R, Nadler JL, Kumar D, Kalra VK. Glucose induces lipid peroxidation and inactivation of membrane-associated ion-transport enzymes in human erythrocytes in vivo and in vitro. *J Cell Physiol*. Published online. 1991;149(1):100-109. https://doi.org/10.1002/jcp.1041490113
49. Manohar SM, Vaikasuvu SR, Deepthi K, Sachan A, Narasimha SRPVL. An association of hyperglycemia with plasma malondialdehyde and atherogenic lipid risk factors in newly diagnosed type 2 diabetic patients. *J Res Med Sci*. Published online. 2013;18(2):89-93.
50. Yagi K. Simple assay for the level of total lipid peroxides in serum or plasma. *Methods Mol Biol*. Published online. 1998;108:101-106. https://doi.org/10.1385/0-89603-472-0:101
51. Laemmli UK. Cleavage of structural proteins during the assembly of the head of bacteriophage T4. *Nature*. Published online. 1970;227(5259):680-685. https://doi.org/10.1038/227680a0
52. Towbin H, Staehelin T, Gordon J. Electrophoretic transfer of proteins from polyacrylamide gels to nitrocellulose sheets: procedure and some applications. *Proc Natl Acad Sci U S A*. Published online. 1979;76(9):4350-4354. https://doi.org/10.1073/pnas.76.9.4350
53. Wang X, Gao Y, Tian N, et al. Astragaloside IV inhibits glucose-induced epithelial-mesenchymal transition of podocytes through autophagy enhancement via the SIRT–NF-κB p65 axis. *Sci Rep*. 2019;9(1):1-11. https://doi.org/10.1038/s41598-018-36911-1
54. Capone V, Clemente E, Restelli E, et al. PERK inhibition attenuates the abnormalities of the secretory pathway and the increased apoptotic rate induced by SIL1 knockdown in HeLa cells. *Biochim Biophys Acta - Mol Basis Dis*. Published online. 2018;1864(10):3164-3180. https://doi.org/10.1016/j.bbadis.2018.07.003
55. Boncompagni S, Rossi AE, Micaroni M, et al. Characterization and temporal development of cores in a mouse model of malignant hyperthermia. *Proc Natl Acad Sci U S A*. Published online. 2009;106(51):21996-22001. https://doi.org/10.1073/pnas.0911496106
56. Debacq-Chainiaux F, Erusalimsky JD, Campisi J, Toussaint O. Protocols to detect senescence-associated beta-galactosidase (SA-βgal) activity, a biomarker of senescent cells in culture and in vivo. *Nat Protoc*. Published online. 2009;4(12):1798-1806. https://doi.org/10.1038/nprot.2009.191
57. Baskin SI, Salem H. *Oxidants, Antioxidants, and Free Radicals*. 2017. https://doi.org/10.1201/9780203744673
58. De Haan JB, Cristiano F, Iannello RC, Kola I. Cu/Zn-superoxide dismutase and glutathione peroxidase during aging. *Biochem Mol Biol Int*. Published online. 1995;35(6):1281-1297.
59. Amicarelli F, Colafarina S, Cattani F, et al. Scavenging system efficiency is crucial for cell resistance to ROS-mediated methylglyoxal injury. *Free Radic Biol Med*. Published online. 2003;35(8):856-871. https://doi.org/10.1016/S0891-5849(03)00438-6
60. Nishikawa T, Araki E. Impact of mitochondrial ROS production in the pathogenesis of diabetes mellitus and its complications. *Antioxid Redox Signal*. Published online. 2007;9(3):343-353. https://doi.org/10.1089/ars.2006.1458
61. Sivandzade F, Bhalerao A, Cucullo L. Analysis of the mitochondrial membrane potential using the cationic JC-1 dye as a sensitive fluorescent probe. *Bio-Protocol*. 2019;9(1):1-13. https://doi.org/10.21769/bioprotoc.3128
62. Cossarizza A, Ceccarelli D, Masini A. Functional heterogeneity of an isolated mitochondrial population revealed by cytofluorometric analysis at the single organelle level. *Exp Cell Res*. Published online. 1996;222(1):84-94. https://doi.org/10.1006/excr.1996.0011
63. Marchetti C, Jouy N, Leroy-Martin B, Defossez A, Formstecher P, Marchetti P. Comparison of four fluorochromes for the detection of the inner mitochondrial membrane potential in human spermatozoa and their correlation with sperm motility. *Hum Reprod*. Published online. 2004;19(10):2267-2276. https://doi.org/10.1093/humrep/deh416
64. Seo AY, Joseph AM, Dutta D, Hwang JCY, Aris JP, Leeuwenburgh C. New insights into the role of mitochondria in aging: mitochondrial dynamics and more. *J Cell Sci*. Published online. 2010;123(15):2533-2542. https://doi.org/10.1242/jcs.070490
65. Berridge MV, Herst PM, Tan AS. Tetrazolium dyes as tools in cell biology: new insights into their cellular reduction. *Biotechnol Annu Rev*. Published online. 2005;11:127-152. https://doi.org/10.1016/S1387-2656(05)11004-7
66. Yessoufou A, Moutairou K. Maternal diabetes in pregnancy: early and long-term outcomes on the offspring and the concept of "metabolic memory". *Exp Diabetes Res*. 2011;2011:1-12. https://doi.org/10.1155/2011/218598
67. Ozuguz U, Isik S, Berker D, et al. Gestational diabetes and subclinical inflammation: evaluation of first year postpartum outcomes. *Diabetes Res Clin Pract*. 2011;94(3):426-433. https://doi.org/10.1016/j.diabres.2011.08.024
68. Sobrevia L, Salsoso R, Sáez T, Sanhueza C, Pardo F, Leiva A. Insulin therapy and fetoplacental vascular function in gestational diabetes mellitus. *Exp Physiol*. 2015;100(3):231-238. https://doi.org/10.1113/expphysiol.2014.082743

69. Villalobos-Labra R, Westermeier F, Pizarro C, et al. Neonates from women with pregestational maternal obesity show reduced umbilical vein endothelial response to insulin. *Placenta*. 2019;86(April):35-44. https://doi.org/10.1016/j.placenta.2019.07.007
70. Katsuumi G, Shimizu I, Yoshida Y, Minamino T. Vascular senescence in cardiovascular and metabolic diseases. *Front Cardiovasc Med*. 2018;5(March):1-13. https://doi.org/10.3389/fcvm.2018.00018
71. Ucci M, Di Tomo P, Tritschler F, et al. Anti-inflammatory role of carotenoids in endothelial cells derived from umbilical cord of women affected by gestational diabetes mellitus. *Oxid Med Cell Longev*. 2019;2019:1-11. https://doi.org/10.1155/2019/8184656
72. Feng Y, Chu A, Luo Q, Wu M, Shi X, Chen Y. The protective effect of astaxanthin on cognitive function via inhibition of oxidative stress and inflammation in the brains of chronic T2DM rats. *Front Pharmacol*. 2018;9:1-11. https://doi.org/10.3389/fphar.2018.00748
73. Mathur A, Hong Y, Kemp BK, Barrientos AA, Erusalimsky JD. Evaluation of fluorescent dyes for the detection of mitochondrial membrane potential changes in cultured cardiomyocytes. *Cardiovasc Res*. Published online. 2000;46(1):126-138. https://doi.org/10.1016/S0008-6363(00)00002-X
74. Masoud S, McDonald F, Bister D, Kotecki C, Bootman MD, Rietdorf K. Examining cardiomyocyte dysfunction using acute chemical induction of an ageing phenotype. *Int J Mol Sci*. 2020;21(1):197. https://doi.org/10.3390/ijms21010197
75. Fiorentino T, Prioletta A, Zuo P, Folli F. Hyperglycemia-induced oxidative stress and its role in diabetes mellitus related cardiovascular diseases. *Curr Pharm Des*. 2013;19(32):5695-5703. https://doi.org/10.2174/1381612811319320005
76. Chen J, Goligorsky MS. Premature senescence of endothelial cells: Methusaleh's dilemma. *Am J Physiol Heart Circ Physiol*. 2006;290(5):H1729-H1739. https://doi.org/10.1152/ajpheart.01103.2005
77. Alessio N, Capasso S, Ferone A, et al. Misidentified human gene functions with mouse models: the case of the retinoblastoma gene family in senescence. *Neoplasia (United States)*. 2017;19(10):781-790. https://doi.org/10.1016/j.neo.2017.06.005
78. Gui J, Potthast A, Rohrbach A, Borns K, Das AM, Von Versen-Hoynck F. Gestational diabetes induces alterations of sirtuins in fetal endothelial cells. *Pediatr Res*. 2016;79(5):788-798. https://doi.org/10.1038/pr.2015.269
79. Yang J, Wang N, Zhu Y, Feng P. Roles of SIRT1 in high glucose-induced endothelial impairment: association with diabetic atherosclerosis. *Arch Med Res*. 2011;42(5):354-360. https://doi.org/10.1016/j.arcmed.2011.07.005
80. Chen Y, Wang Y, Jiang Y, Zhang X, Sheng M. High-glucose treatment regulates biological functions of human umbilical vein endothelial cells via Sirt1/FOXO3 pathway. *Ann Transl Med*. 2019;7(9):199. https://doi.org/10.21037/atm.2019.04.29
81. Iskender H, Dokumacioglu E, Sen TM, Ince I, Kanbay Y, Saral S. The effect of hesperidin and quercetin on oxidative stress, NF-κB and SIRT1 levels in a STZ-induced experimental diabetes model. *Biomed Pharmacother*. 2017;90:500-508. https://doi.org/10.1016/j.biopha.2017.03.102

How to cite this article: Di Tomo P, Alessio N, Falone S, et al. Endothelial cells from umbilical cord of women affected by gestational diabetes: A suitable in vitro model to study mechanisms of early vascular senescence in diabetes. *The FASEB Journal*. 2021;35:e21662. https://doi.org/10.1096/fj.202002072RR